

A *Chandra* SNAPSHOT SURVEY FOR 3C RADIO GALAXIES WITH REDSHIFTS BETWEEN 0.3 AND 0.5F. MASSARO¹, D. E. HARRIS², G. R. TREMBLAY³, E. LIUZZO⁴, A. BONAFEDE⁵, A. PAGGI².

version September 11, 2018: fm

ABSTRACT

This paper contains an analysis of short *Chandra* observations of 19 3C sources with redshifts between 0.3 and 0.5 not previously observed in the X-rays. This sample is part of a project to obtain *Chandra* data for all of the extragalactic sources in the 3C catalogue. Nuclear X-ray intensities as well as any X-ray emission associated with radio jet knots, hotspots or lobes have been measured in 3 energy bands: soft, medium and hard. Standard X-ray spectral analysis for the 4 brightest nuclei has been also performed. X-ray emission was detected for all the nuclei of the radio sources in the current sample with the exception of 3C 435A. There is one compact steep spectrum (CSS) source while all the others are FR II radio galaxies. X-ray emission from two galaxy clusters (3C 19 and 3C 320); from 6 hotspots in 4 radio galaxies (3C 16, 3C 19, 3C 268.2, 3C 313); and extended X-ray emission on kpc scales in 3C 187 and 3C 313, has been detected.

Subject headings: galaxies: active — X-rays: general — radio continuum: galaxies

1. INTRODUCTION

The revised version of the Third Cambridge (3C) catalog presented in Spinrad et al. (1985) lists 298 extragalactic radio sources (see also Edge et al. 1959; Mackay 1971, for additional information). In recent years, the large majority of these sources has been observed with several photometric and spectroscopic snapshot surveys approaching the statistical completeness of the 3C (radio flux limited) sample. The Hubble Space Telescope (HST) already completed an optical snapshot survey of the 3C sources at redshift lower than 0.3 (e.g., Chiaberge et al. 2000; Tremblay et al. 2009, and reference therein) while ground based spectroscopic observations have been carried out with the Galileo Telescope (Buttiglione et al. 2009). In addition, radio images with arcsecond resolution for the majority of the 3C sources are available from the NRAO VLA Archive Survey (NVAS)⁶ and in the archives of the Very Large Array (VLA) and MERLIN observatories. Recently, a piecemeal approach of obtaining *Chandra* observations for all the 3C extragalactic sources below redshift 0.3 was completed (Massaro et al. 2010; Massaro et al. 2012, hereinafter Paper I and Paper 2, respectively). *Chandra* is the only X-ray facility with angular resolution comparable to that at optical and radio frequencies.

In this paper we provide source parameters for 19 previously unobserved (by *Chandra*) 3C sources with redshifts between 0.3 and 0.5. With these data, the *Chandra* coverage of 3CR sources with $z < 0.5$ is complete except for the following: one quasar, 3 unclassified sources,

and 1 FR II radio galaxy which had no redshift listed in Spinrad et al. (1985). We plan to include all of these in our next *Chandra* Snapshot proposal. Our eventual goal is to have observations of all 3C extragalactic sources in the *Chandra* archives. As has been amply demonstrated by the observations of sub samples (Cycle 9 and Cycle 12) even with relatively short exposures, almost all nuclei and occasionally X-ray emission associated with jet knots, hotspots, lobes, and hot thermal gas (i.e. ICM of groups or clusters of galaxies) have been clearly detected.

The whole 3CR sample (Spinrad et al. 1985) contains 158 FR II radio galaxies, 39 FR I radio galaxies, 57 quasars, 2 Seyfert galaxies, 2 BL Lacs, 20 unidentified, and 20 unclassified sources. Of these, 74 are still unobserved by *Chandra* and to the best of our knowledge, 26 have no redshift (see Appendix A for specifics).

In Paper I, data reduction and analysis procedures, developed for this project, were presented together with the results for the first 30 radio sources. In Paper II, a similar investigation of an additional 27 sources, to complete the sample to $z \leq 0.3$ has been carried out.

The paper is organized as follows: a brief description of the observations and data reduction procedures is given in § 2 while source details are given in § 3. Then, § 4 is devoted to our summary and conclusions.

For numerical results, cgs units are used unless stated otherwise and a flat cosmology was assumed with $H_0 = 72 \text{ km s}^{-1} \text{ Mpc}^{-1}$, $\Omega_M = 0.27$ and $\Omega_\Lambda = 0.73$ (Dunkley et al. 2009). Spectral indices, α , are defined by flux density, $S_\nu \propto \nu^{-\alpha}$.

2. OBSERVATIONS, DATA REDUCTION, AND BASIC PARAMETERS

Data reduction and data analysis procedures have been extensively described in Paper I and II, thus only the basic details are reported here.

The 3C source sample observed during Cycle 13 is listed in Table 1 together with their salient parameters. Each source was observed for a nominal 12 ksec, and the actual livetimes are given in Table 2, together with the nuclear X-ray fluxes. It is worth noting that in Cycle 13 the *Chandra* exposure time per single source has

¹ SLAC National Laboratory and Kavli Institute for Particle Astrophysics and Cosmology, 2575 Sand Hill Road, Menlo Park, CA 94025, USA.

² Smithsonian Astrophysical Observatory, 60 Garden Street, Cambridge, MA 02138, USA.

³ European Southern Observatory, Karl-Schwarzschild-Str. 2, 85748 Garching bei Muenchen, Germany.

⁴ Istituto di Radioastronomia, INAF, via Gobetti 101, 40129, Bologna, Italy.

⁵ Hamburger Sternwarte, Universität Hamburg, Gojenbergsweg 112, 21029 Hamburg, Germany.

⁶ <http://www.aoc.nrao.edu/~vlbacald/>

been increased by 50% with respect to the previous 3C snapshot survey carried out in Cycles 9 and 12 observed with 8 ksec nominal exposure. The ACIS-S back illuminated chip in VERY FAINT mode with standard frame times (3.2s) has been used. All the observations had 4 chips turned on: I2, I3, S2, and S3. The data reduction has been performed following the standard reduction procedure described in the *Chandra* Interactive Analysis of Observations (CIAO) threads⁷, using CIAO v4.4 and the *Chandra* Calibration Database (CALDB) version 4.5.3.

Level 2 event files were generated using the *acis_process_events* task and events were filtered for grades 0,2,3,4,6. Lightcurves were also extracted for every dataset to verify the absence of high background intervals. Astrometric registration was achieved by changing the appropriate keywords in the fits header so as to align the nuclear X-ray position with that of the radio (see Section 2 in Paper II).

2.1. Fluxmaps

Three different fluxmaps were created in the energy ranges: 0.5 – 1 keV (soft), 1 – 2 keV (medium), 2 – 7 keV (hard), by filtering the event file with the appropriate energy range and dividing the data with monochromatic exposure maps (with nominal energies of soft=0.8keV, medium=1.4keV, and hard=4keV).

To recover the angular resolution of the Chandra mirrors, the undersampling imposed by the ACIS pixel size was avoided by regridding to obtain pixel sizes of 0.123'' or smaller. For sources of large angular extent 1/2 or no regridding was used.

To obtain maps with brightness units of $\text{ergs cm}^{-2} \text{ s}^{-1} \text{ pixel}^{-1}$, each event was multiplied by the nominal energy of its respective band (see Section 2.1 of Paper II for additional details).

To measure observed fluxes for any feature, an appropriate region (usually circular) was chosen. For the nuclei, regions of 2'' radius have been used while for other features the size is given in Table 3. For each feature, background circular regions, with the same size described above, were chosen so as to avoid contaminating X-ray emission (and also radio emission) and to sample both sides of jet features or two areas close to hotspots. X-ray fluxes measured for the nuclei are given in Table 2 while those of the hotspots and knots in Table 3.

2.2. Fluxes for the two nuclei affected by pileup

Two of the detected nuclei had count rates exceeding the adopted pileup threshold of 0.2 counts per frame (see Section 2.3 in Paper II). These are 3C 327.1 (0.45 counts/frame) and 3C 411 (0.75 counts/frame). Since pileup serves to move events to higher energies, it was not possible to use fluxmaps to measure fluxes in the 3 bands. Instead, the *jdpileup* spectral fitting was adopted (§ 2.3) to determine the appropriate fluxes. In addition the “light bucket” method developed for the M87 jet (Harris et al. 2006) to obtain a rough estimate of the total flux has been also used. The energies of all source events in the evt1 file (i.e. no grade filtering so as to recover events rejected in evt2 files because of grade migration) from 0.5 to some high energy such as 11 or 14 keV

(determined by inspection) have been summed. Converting the resulting values of keV/s to cgs is a very inaccurate process since it is not possible to know the effective area for each of the photons comprising a piled event. Adopting a global effective area of 480 cm^2 should provide a reasonable flux estimate unless these nuclei have an intrinsic spectrum much harder than that of the knot HST-1 in the M87 jet. If that were to be the case, we should have used a smaller effective area, and our fluxes using 480 cm^2 would be lower limits.

2.3. X-ray Spectral Analysis of the stronger nuclei

As already done for the 3C sources observed by *Chandra* in Cycles 9 and 12, the X-ray spectral analysis for the nuclei containing 250 or more counts was performed to estimate their X-ray spectral indices α_X and the presence or absence of significant intrinsic absorption $N_H(z)$. The spectral analysis was carried out using the XSPEC version 12.6 software package (Arnaud 1996).

The spectral data were extracted from a 1''.5 aperture using the CIAO 4.4 routine *specextract*, thereby automating the creation of count-weighted response matrices. The background-subtracted spectra were then filtered in energy between 0.3-7 keV, and binned to a minimum of 30 counts per bin to ensure the validity of χ^2 statistics.

Each source was fitted with two multiplicative models: (1) a simple redshifted powerlaw with Galactic and intrinsic photoelectric absorption components (*phabs*×*zphabs*×*zpowerlaw* in XSPEC syntax), and (2) the same model with an additional pileup component, (*pileup*×*phabs*×*zphabs*×*zpowerlaw*), using the XSPEC implementation of the *Chandra* pileup model described by Davis (2001). The grade migration parameter was set to unity. For the two piled sources (3C 327.1 and 3C 411), the values of α_x for the *jdpileup* model are significantly larger (and are to be preferred) than the values from the standard fits.

Prior to fitting, the Milky Way hydrogen column density (Kalberla et al. 2005) and the source redshift were fixed to the values reported in Table 1. The two main variable parameters, namely the intrinsic absorption $N_H(z)$ and X-ray spectral index α_X were allowed to vary in a first pass fit, but subsequently stepped through a range of possible physical values to explore the parameter space, determine 90% confidence intervals, and quantify the degree to which $N_H(z)$ and α_X are degenerate. Monte Carlo Markov Chains were created to further aid our understanding of these behaviors. It is worth noting that those sources with inverted best-fit spectral indices ($\alpha_X < 0$) can result from Compton Thick models. Results are reported in Table 4.

2.4. Photometric estimates of the intrinsic absorption

Due to the relatively short exposure times of the *Chandra* snapshot survey, it is not often possible to recover the parameters of interest (α_X and $N_H(z)$) from the spectral fits but it is possible to derive a range of intrinsic $N_H(z)$ column densities corresponding to some chosen range in α_X by using simulated spectra. Thus, as already investigated in Paper I and II, a photometric analysis was performed to estimate the intrinsic absorption $N_H(z)$.

⁷ <http://cxc.harvard.edu/ciao/guides/index.html>

TABLE 1
SOURCE LIST OF THE *Chandra* CYCLE 13 SNAPSHOT SURVEY OF 3C RADIO SOURCES WITH $0.3 < z < 0.5$

3C	Class ^(a)	R.A. (J2000) ^(b) hh mm ss	Dec. (J2000) ^(b) dd mm ss	z ^(c)	D_L (Mpc)	Scale (kpc/'')	$N_{H,Gal}$ ^(d) (cm ⁻²)	m_v ^(e)	S_{178} ^(f) (Jy)	<i>Chandra</i> Obs ID	Obs. Date yyyy-mm-dd
16	FR II - HEG	00 37 45.40	+13 20 09.2	0.405	2161.8	5.309	4.58e20	21.0	11.2	13879	2012-10-25
19	FR II - LEG	00 40 54.99	+33 10 07.1	0.482	2662.9	5.878	6.18e20	20.0	12.1	13880	2011-10-29
42	FR II - HEG	01 28 30.12	+29 03 00.8	0.395	2098.5	5.228	6.42e20	20.0	12.0	13872	2012-02-26
46	FR II - HEG	01 35 28.48	+37 54 05.2	0.437	2369.1	5.560	5.64e20	19.5	10.2	13881	2012-09-28
67	CSS - BLO	02 24 12.29	+27 50 11.5	0.310	1579.7	4.462	7.47e20	18.0	10.0	13873	2011-11-27
103	FR II - ?	04 08 03.10	+43 00 32.7	0.330	1697.9	4.654	3.18e21	19.0	26.6	13874	2012-11-10
187	FR II - ?	07 45 04.46	+02 00 08.7	0.350	1819.2	4.839	6.00e20	19.5	8.1	13875	2012-01-04
244.1	FR II - HEG	10 33 33.98	+58 14 35.7	0.428	2308.9	5.489	6.67e19	19.0	20.3	13882	2013-01-17
268.2	FR II - ?	12 00 58.61	+31 33 19.9	0.362	1892.8	4.947	1.64e20	19.0	9.7	13876	2012-07-07
274.1	FR II - ?	12 35 26.66	+21 20 34.8	0.422	2270.3	5.443	2.35e20	20.0	16.5	13883	2011-11-06
275	FR II - LEG	12 42 19.89	-04 46 20.1	0.480	2649.6	5.864	1.86e20	21.0	14.5	13884	2012-07-12
306.1	FR II - HEG	14 55 01.40	-04 20 59.8	0.441	2393.1	5.587	6.11e20	19.0	13.5	13885	2012-09-06
313	FR II - HEG	15 11 00.03	+07 51 50.1	0.461	2523.9	5.732	2.40e20	21.0	20.6	13886	2012-05-07
320	FR II - ?	15 31 25.37	+35 33 40.0	0.342	1770.5	4.766	1.69e20	18.0	9.1	13877	2011-12-02
327.1	? - HEG	16 04 45.38	+01 17 50.3	0.462	2530.4	5.740	6.40e20	20.5	23.6	13887	2012-05-08
341	FR II - HEG	16 28 03.98	+27 41 39.3	0.448	2438.7	5.639	3.51e20	19.0	10.8	13888	2011-11-14
411	FR II - HEG	20 22 08.44	+10 01 11.3	0.467	2563.4	5.775	1.06e21	19.7	16.5	13889	2012-08-08
434	FR II - ?	21 23 16.24	+15 48 05.8	0.322	1649.9	4.577	6.57e20	20.8	4.8	13878	2012-08-15
435B	FR II - ?	21 29 06.10	+07 32 54.8	0.865	5460.0	7.610	4.44e20	19.4	—	13890	2012-08-14

(a) The ‘class’ column contains both a radio descriptor (Fanaroff-Riley class I or II), Compact Steep Spectrum (CSS) and the optical spectroscopic designation, LEG, “Low Excitation Galaxy”, HEG, “High Excitation Galaxy”, and BLO, “Broad Line Object”. The symbol “?” indicates those radio and optical classifications that are uncertain or not reported in the literature.

(b) The celestial positions listed are those of the radio nuclei which we used to register the X-ray images except for the 4 sources lacking an obvious radio nucleus. For these four (3C 16, 3C 19, 3C 268.2, and 3C 275) we use Spinrad’s position (Spinrad et al. 1985). For 3C 275 the listed position falls a few arcsec E of the radio and X-ray emission.

(c) Redshift measurements are taken from Spinrad et al. (1985) or from NASA/IPAC Extragalactic Database (NED) for 3C 435B.

(d) Galactic Neutral hydrogen column densities $N_{H,Gal}$ are taken from Kalberla et al. (2005).

(e) m_v is the visual magnitude (Spinrad et al. 1985) or from NASA/IPAC Extragalactic Database (NED) for 3C 435B.

(f) S_{178} is the flux density at 178 MHz, taken from Spinrad et al. (1985).

This study is based on the values of the hardness ratios HR (see § 3.1) derived from the photometric analysis of the nuclear X-ray fluxes.

The observed nuclear fluxes have been used to determine the hardness ratios HR according to the simple relation: $(H - M)/(H + M)$, where H and M are the X-ray fluxes in the hard and the medium bands, respectively. The uncertainties on the observed values of HR , have been derived from the X-ray flux errors. We did not use the soft X-ray band because it is the band most affected by absorption, often leading to a low number of soft counts.

Most nuclei of radio galaxies show X-ray spectra well described by a simple power law model with α_X values ranging between 0.5 and 1.5 or occasionally larger (e.g. Hardcastle et al. 2009; Worrall et al. 2009). Numerical simulations with XSPEC were performed to derive the values of $N_H(z)$ in the case of an intrinsically absorbed power-law spectrum with different values of the spectral index α_X and source redshift z corresponding to different values of the hardness ratio to derive the relation between the $N_H(z)$ and observed HR . We iterate this procedure for two values of α_X corresponding to 0.5 and 1.5. In this photometric analysis we adopted a more restricted energy range of α_X with respect to that used in the X-ray spectral analysis (see notes to Table 4). However, this restricted range of α_X values is in agreement with previous investigations (i.e., Paper II) and with the distribution of the spectral index of the low redshift 3C radio sources (e.g., Hardcastle et al. 2009). In Figure 1, the N_H versus HR curves for 3C 275 with $\alpha_X=0.5$ and $\alpha_X=1.5$ are shown.

The N_H estimates corresponding to the observed HR , including 1σ error, were calculated for the two values of α_X reported above in each source (see Figure 1 for additional details). Then, the maximum and the minimum values of these $N_H(z)$ estimates were considered to define the range where the ‘real’ $N_H(z)$ value could be, corresponding to an estimate of the error on the $N_H(z)$. The ranges derived for each HR value are reported in Table 2.

It is worth noting that if a generic source is Compton thick (i.e., $N_H(z) > 10^{24}$ cm⁻²) or if its X-ray spectrum is inverted (i.e. $\alpha_X < 0$) the hardness ratios cannot provide a reliable estimate of absorption. For a more detailed discussion of the photometric absorption analysis see Section 3.2 of Paper 2.

Finally, the results obtained from the HR study were compared with those derived from the X-ray spectral analysis (see Table 2 in comparison with Table 4). Satisfactory agreement between the two methods was also obtained for the sources in Paper 2 which were bright enough to warrant spectral analysis. No comparison is possible for the two piled sources, 3C327.1 and 3C411. The single case of disagreement occurred for the CSS source 3C67, probably suggesting a more complex X-ray spectrum.

3. RESULTS

3.1. General

X-ray emission was detected for all the nuclei in the sample except for 3C 435A (see § 3.2 for more details). All the X-ray images are presented in Appendix B.

In addition, as performed for the previous subset of

TABLE 2
NUCLEAR X-RAY FLUXES

3C	LivTim ^(a) (ksec)	Net ^(b) (cnts)	Ext. Ratio ^(c)	f(soft) 0.5-1 keV	f(medium) 1-2 keV	f(hard) 2-7 keV	f(total) 0.5-7 keV	HR	N _H (z) ^(d) (10 ²² cm ⁻²)	L _X (10 ⁴² erg s ⁻¹)
16	11.92	2.8(1.7)	0.22(0.15)	0.34(0.34)	—	3.3(2.3)	3.6(2.3)	—	—	2.0(1.3)
19	11.89	35(6)	0.16(0.03)	—	—	24.1(5.6)	24.1(5.6)	<1.00	<36	20.6(4.7)
42	11.92	39(6)	0.78(0.17)	—	0.56(0.56)	46.6(7.8)	47.2(7.8)	0.98(0.23)	4.7 - 25	24.8(4.1)
46	11.92	50(7)	0.81(0.15)	0.79(0.46)	0.88(0.51)	63.5(10.0)	65.2(10.0)	0.97(0.22)	2.8 - 36	43.8(6.7)
67	11.89	567(24)	0.96(0.06)	30.3(3.2)	74.7(4.8)	257(17)	361(18)	0.55(0.06)	1.9 - 5.0	108(5)
103	11.92	241(15)	0.92(0.08)	0.36(0.36)	6.3(1.5)	320(22)	327(22)	0.96(0.09)	6.1 - 25	113(8)
187	11.90	9(3)	0.15(0.05)	0.93(0.53)	—	3.1(2.8)	4.0(2.9)	<1.00	<25	1.6(1.2)
244.1	11.92	44(7)	0.60(0.12)	3.9(1.2)	1.2(0.7)	39.5(7.5)	44.6(7.6)	0.94(0.25)	4.3 - 36	28.4(4.8)
268.2	11.58	12(3)	0.41(0.14)	0.55(0.39)	1.3(0.7)	6.7(3.4)	8.6(3.5)	0.67(0.51)	<25	3.7(1.5)
274.1	11.90	22(4)	0.49(0.12)	—	0.52(0.37)	27.3(6.5)	27.8(6.5)	0.96(0.33)	3.5 - 36	17.2(4.0)
275	12.41	45(6)	0.80(0.16)	0.88(0.51)	4.0(1.1)	30.1(5.8)	35.0(5.9)	0.77(0.22)	3.0 - 29.4	29.4(5.0)
306.1	11.92	24(5)	0.63(0.16)	0.55(0.39)	—	27.9(6.3)	28.5(6.3)	<1.00	<36	19.5(4.3)
313	11.92	24(5)	0.57(0.15)	—	—	33.7(6.7)	33.7(6.7)	<1.00	<37	25.7(5.3)
320	11.90	68(8)	0.13(0.02)	6.1(1.7)	5.3(1.7)	14.9(5.3)	26.3(5.8)	0.48(0.30)	<7.3	9.9(2.2)
327.1 ^(e)	11.11	1235(35)	0.90(0.04)	96(10)	204(20)	935(94)	1236(97)	—	—	946(74)
341	11.64	18(4)	0.64(0.19)	0.59(0.59)	1.46(0.73)	13.9(4.2)	16.0(4.3)	0.81(0.36)	2.0 - 36	11.3(3.1)
411 ^(e)	11.91	1716(41)	0.93(0.03)	116(11)	279(31)	1627(155)	2023(158)	—	—	1590(120)
434	11.92	44(7)	0.83(0.17)	4.2(1.2)	6.1(1.4)	15.2(4.4)	25.5(4.8)	0.43(0.24)	<5.7	8.3(1.6)
435B	11.92	293(17)	0.90(0.07)	5.6(1.4)	38.0(3.5)	179(14)	223(15)	0.65(0.08)	3.2 - 8.4	795(43)

NOTE. — Fluxes are given in units of 10⁻¹⁵erg cm⁻²s⁻¹. Values in parentheses are 1 σ uncertainties.

^aLivTim is the live time

^bNet is the net counts within a circle of radius=2''.

^cExt. Ratio ("Extent Ratio") is the ratio of the net counts in the r=2'' circle to the net counts in the r=10'' circle. Values significantly less than 0.9 indicate the presence of extended emission around the nuclear component (see Section 3.1).

^dAs per the discussion in the text, the value of N_H (z), required to produce the observed HR values, was computed. The uncertainty given here is indicative only: it is the range of N_H (z) covered by the uncertainty in the HR and allowing α_X to range from 0.5 to 1.5. Obviously there may be some sources with intrinsic spectral indices outside of this range.

^eFor 3C 327.1 and 3C 411, X-ray fluxes and luminosities have been computed via spectral fitting including the jdpileup model (see § 2.3 for more details), thus the N_H (z) values are reported in Table 4. The 'light bucket' estimates of the total flux (§ 2.2) are in reasonable agreement with those in the table: 1050 (3C 327.1) and 2120 (3C 411).

TABLE 3
RADIO COMPONENTS WITH X-RAY DETECTIONS

3C	Component ^a	Radius ^b (arcsec)	counts (bkg) ^c	Detection Significance ^d	f _{0.5-1 keV} (cgs)	f _{1-2 keV} (cgs)	f _{2-7 keV} (cgs)	f _{0.5-7 keV} (cgs)	L _X 10 ⁴² erg s ⁻¹
16	<i>l</i> - n 11.1	3.0	5(2)	2.1 σ	—	0.44(0.44)	1.37(1.37)	1.81(1.44)	1.01(0.80)
	<i>l</i> - n 5.2	2.5	3(1)	2.0 σ	0.36(0.36)	0.22(0.22)	—	0.58(0.42)	0.32(0.24)
	<i>l</i> - s 6.0	3.0	2(1)	1.4 σ	0.37(0.37)	0.12(0.27)	—	0.50(0.46)	0.28(0.26)
	<i>h</i> - s 22.8	3.0	4(1)	2.7 σ	0.40(0.40)	0.49(0.35)	—	0.89(0.53)	0.50(0.30)
19	<i>h</i> - n 3.0	0.8	5(1)	3.2 σ	0.39(0.39)	0.73(0.53)	0.93(0.93)	2.05(1.14)	1.74(0.96)
	<i>h</i> - s 3.5	0.8	6(2)	2.5 σ	0.88(0.51)	0.78(0.67)	1.74(1.23)	3.40(1.49)	2.88(1.26)
187	<i>l</i> - n 37.0	12.0	46(11)	>7.0 σ	4.02(1.30)	5.25(1.43)	2.37(2.37)	11.64(3.06)	4.61(1.21)
	<i>l</i> - n 75.0	12.0	30(5)	>7.0 σ	1.27(0.69)	1.16(0.63)	7.98(3.62)	10.41(3.74)	4.12(1.48)
	<i>l</i> - s 27.0	12.0	46(13)	>7.0 σ	2.86(1.31)	5.41(1.42)	7.19(4.64)	15.46(5.03)	6.12(1.99)
	<i>l</i> - s 60.0	15.0	56(15)	>7.0 σ	1.57(0.70)	2.51(1.06)	2.49(2.49)	6.57(2.80)	2.60(1.11)
268.2	<i>h</i> - s 46.0	2.0	2(1)	1.4 σ	0.38(0.38)	0.14(0.14)	—	0.52(0.40)	0.22(0.17)
313	<i>h</i> - e 73.0	1.5	4(1)	2.7 σ	—	0.53(0.37)	2.26(1.59)	2.79(1.63)	2.13(1.24)
	<i>h</i> - w 55.0	1.5	5(1)	3.2 σ	0.76(0.54)	0.22(0.22)	1.67(1.67)	2.64(1.77)	2.02(1.35)
327.1	<i>k</i> - s 3.3	2.7x1	9(3)	3.0 σ	0.01(0.01)	2.17(0.90)	—	2.18(0.90)	1.67(0.69)
	<i>k</i> - s 5.0	0.8	3(1)	2.0 σ	—	0.69(0.49)	—	0.69(0.49)	0.53(0.38)
341	<i>k</i> - w 8.0	1.5	3(1)	2.0 σ	0.78(0.55)	—	0.98(0.98)	1.76(1.12)	1.25(0.80)

Fluxes are given in units of 10⁻¹⁵erg cm⁻²s⁻¹.

(a) The component designation is comprised of a letter indicating the classification (i.e., knot *k*, hotspot *h*, lobe *l*), a cardinal direction (as viewed from the nucleus) plus the distance from the nucleus in arcseconds.

(b) The radius column gives the size of the aperture used for photometry.

(c) The counts column gives the total counts in the photometric circle together with those measured in the background regions of the same area, in parentheses; both for the 0.5 to 7 keV band.

(d) The confidence level of each detection evaluated adopting a Poisson distribution.

TABLE 4
SPECTRAL ANALYSIS OF BRIGHT NUCLEI

Source (1)	α_X (2)	$N_H(z)$ ($\times 10^{22} \text{ cm}^{-2}$) (3)	χ^2/dof (4)
3C 67	$[0.32^{+0.27}_{-0.25}]$ $[0.51^{+0.31}_{-0.29}]$	$0.26^{+0.13}_{-0.11}$ $0.32^{+0.14}_{-0.12}$	8.74/15 8.62/15
3C 327.1	$0.25^{+0.13}_{-0.09}$ $0.81^{+0.18}_{-0.17}$	$0.025^{+0.13}_{-0.12}$ $0.16^{+0.15}_{-0.14}$	42.7/38 41.5/38
3C 411	$0.11^{+0.06}_{-0.06}$ $1.01^{+0.16}_{-0.16}$	$[0.00^{+0.05}]$ $0.18^{+0.12}_{-0.11}$	55.3/60 47.2/60
3C 435B	$0.96^{+0.28}_{-0.28}$ $1.07^{+0.30}_{-0.30}$	$[3.0^{+1.9}_{-1.7}]$ $[3.1^{+1.9}_{-1.8}]$	6.38/6 6.33/6

These 4 nuclei have 250 or more counts and are thus suitable for spectral analysis. The first row for each source is the result for a simple power law fit with galactic and intrinsic absorption. The second row is for the same model with the addition of ‘jdpileup’. For these fits, the corresponding range of best-fit N_H as the spectral index α_X is stepped through values of 0.0 to 2.0 are shown in square brackets. Column (1): source name. Column (2): X-ray spectral index α_X . Column (3): intrinsic absorbing column density in units of 10^{22} cm^{-2} . Column (4): χ^2 / degrees of freedom.

3C sources observed during the *Chandra* Cycle 9 and 12, the net number of counts within circular regions of radii $2''$ and $10''$ was measured, both centered on the nucleus of each source. In Table 2 the $r=2''$ result together with the ratio of r_2/r_{10} are listed, a diagnostic for the presence of extended emission around the nucleus. The only exceptions are 3C 19 and 3C 320 that lie in X-ray detected galaxy clusters (as shown in the figures of Appendix B) and 3C 435A for which the X-ray core is undetected. This ratio should be close to unity for an unresolved (i.e., point-like) sources since the on-axis encircled energy for $r=2''$ is ≈ 0.97 , so we expect only a small increase between $r=2''$ and $r=10''$ for an unresolved source.

Amongst the 19 sources listed in Table 2, there are 10 for which the value of ‘Extent Ratio’ plus its error is < 0.9 , i.e. indicating the presence of extra-nuclear

emission. For 6 of these 10, we have reported features aligned with radio components in Table 3. Of the four remaining, 3C 320 is an obvious cluster of galaxies (see Figure 17 in Appendix B). For the remaining three (3C 244.1, 3C 274.1, and 3C 306.1) we have verified the extended emission by way of heavily smoothed images. There does not appear to be any commonality in the morphologies of the extended features except that none of the 3 display a smooth, circularly symmetric emission. Rather there are irregular clumps of emission, often, but not always along the radio source axis.

In the current sample of 19 X-ray detected sources all are classified as FR II radio galaxies except for 3C 327.1 (uncertain classification) and the CSS source 3C 67. For 3C 16, 3C 19, 3C 268.2, 3C 313 we detect hotspots in the *Chandra* images, with confidence levels between 1.4σ and 3.2σ . In addition, in the cases of 3C 187 and 3C 313 extended X-ray emission, of still uncertain nature, is detected, arising from the regions coincident with, and interior to, their radio lobes (see Figure 2 and Figure 3, and § 3.2 for more details). This extended emission resembles that associated with radio lobes detected in the X-ray observations of high redshift radio galaxies (e.g., Carilli 2003; Smail et al. 2009; Blundell & Fabian 2011, and reference therein). Finally, X-ray emission cospatial with radio knots in the jets of 3C 341 and 3C 327.1, the last resembling the structure of 3C 17 (Massaro et al. 2009), was also detected. Fluxes for jets, hotspots and lobe structures found in the 3C sample are reported in Table 3, where the confidence level of each detection evaluated adopting a Poisson distribution are also provided.

3.2. Source details

3C 16 is an FR II radio galaxy optically classified as HEG. The SW radio lobe is about 16 times the flux density of the NE lobe at 8 GHz and the brightness ratio is between 30 and 40 for arcsec sized beams. From the data available to us, there is no sign of a radio nucleus nor an X-ray component that would indicate the position of the host galaxy or quasar. The original optical identification (Riley et al. 1980) was the brighter of two faint galaxies. Since we see no obvious other candidates on an HST image, we have labelled regions and assigned results assuming that this identification is correct. This source is an example of a double-double restarting jet as suggested by Schoenmakers et al. (2000) and Gilbert et al. (2004). On the heavily smoothed X-ray map, soft X-ray emission was detected roughly aligned with the two linear segments of excess radio brightness within the SW lobe and with the brightest part of the southern hotspot (see Figure 4 in Appendix B). The alignment between X-ray and radio emissions is not accurate, and is difficult to evaluate quantitatively since the maps have not been registered.

3C 19 is an FR II radio galaxy with low excitation emission lines in its optical spectrum. The size of the extended X-ray emission around this source indicates that 3C 19 lies at the center of a galaxy cluster. At this position, we find cluster #10432 in the list compiled by Wen et al. (2012), based on the Sloan Digital Sky Survey. The presence of the galaxy cluster was originally mentioned by Spinrad et al. (1985). Within a circle centered on the source with radius $40''$ ($\sim 235 \text{ kpc}$), we measured 456 ± 24

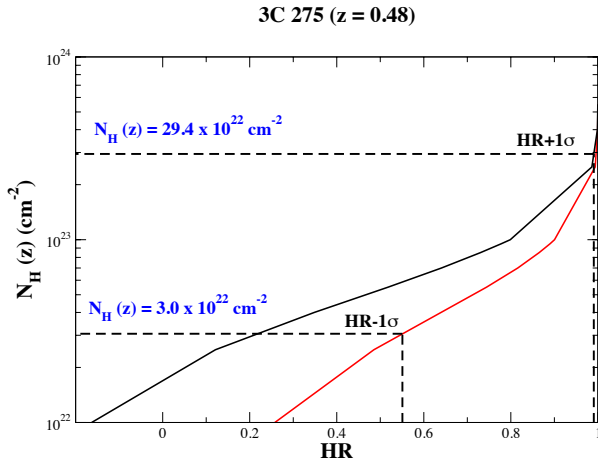


FIG. 1.— The relation between HR and the intrinsic N_H column density resulting from the simulated spectra at redshift 0.48 as for 3C 275 and computed for the case of $\alpha_X = 0.5$ (black solid line) and 1.5 (red solid line).

net counts in the 0.5 - 7 keV energy range. With the current radio maps available to us, it was not possible to locate a radio nucleus; moreover the X-ray core does not appear to be point-like. Thus it was not possible to register the X-ray image to the radio map. Enhanced X-ray brightness associated with the northern hotspot and perhaps also at the southern hotspot has been found, while the axis of the radio and of the X-ray emission is directed almost perpendicular to the optical emission seen by HST (de Koff et al. 1996).

3C 42 is an FR II radio galaxy optically classified as HEG. The X-ray nucleus was clearly detected in the *Chandra* snapshot observation.

3C 46 is an FR II - HEG radio galaxy. There was some uncertainty locating the nucleus for the host galaxy of 3C 46. Examining the low resolution 1.5 GHz radio map, one would confidently identify the nucleus as the weak source between the two lobes. However, at 8.4 GHz with an $0.3''$ beam, there is no detectable emission at this location. Instead, there is an unresolved source (1.9 mJy) $6.7''$ to the south-west, just inside the western lobe and very close to the line joining the southern hotspot to the weak 1.5 GHz source between the lobes. The X-ray core aligns with this 8.4 GHz source. Although it is possible to posit very heavy absorption so as to render the nucleus unobservable in the *Chandra* bandpass, it is puzzling that the nucleus would be detected at 1.5 GHz but not at 8.4 GHz. Of the 51 counts associated with the 8.4 GHz source, only 6 are below 2 keV, with 9 in the 2-4 keV band and 36 between 4 and 7 keV (no counts above 7 keV). For a power law distribution, both the radio and the X-ray spectra would be inverted (i.e., $\alpha < 0$). According to Spinrad et al. (1985) 3C 46 belongs to a galaxy cluster but no extended X-ray emission is detected in the *Chandra* observations.

3C 67 is the only CSS radio source in this sample, and is optically classified as a Broad Line Object (BLO). The bright X-ray nucleus is the only detection. The optical emission revealed by HST is extended in the same direction as the radio axis (de Koff et al. 1996).

3C 187 is a typical FR II radio galaxy. Two unresolved radio sources lie where the radio nucleus is expected to be. They are separated by $2.0''$ in PA= -21° ; i.e. along the principle axis of the radio source. Comparing flux densities at 1.4 GHz and 8.4 GHz, it is clear that the southern source has an inverted spectrum whereas the northern source has a normal spectrum. The southern source is located at RA=07h 45m 04.46s, DEC= $2^\circ 00' 08.7''$ with flux densities $S_{1.4}=0.9$ mJy and $S_{8.4}=3.3$ mJy. The northern radio source has $S_{1.4}=0.9$ mJy and $S_{8.4}=0.4$ mJy. The nucleus is not well defined in the X-rays; there are only two counts above 2 keV coincident with the southern source. In the heavily smoothed X-ray map (see Figure 2) significant X-ray emission from both the northern and the southern lobes appears; 431 ± 27 net counts were found between 0.5 and 7 keV, mostly below 2 keV within a rectangular region $170'' \times 75''$ (PA= -21°) with two background regions of the same size deployed on either side.

3C 244.1 The fact that the soft flux is significantly larger than the medium flux suggests the presence of a soft excess. On the other hand, no extended emission arising from its surrounding galaxy cluster (Hill & Lilly 1991) is seen in the *Chandra* observation.

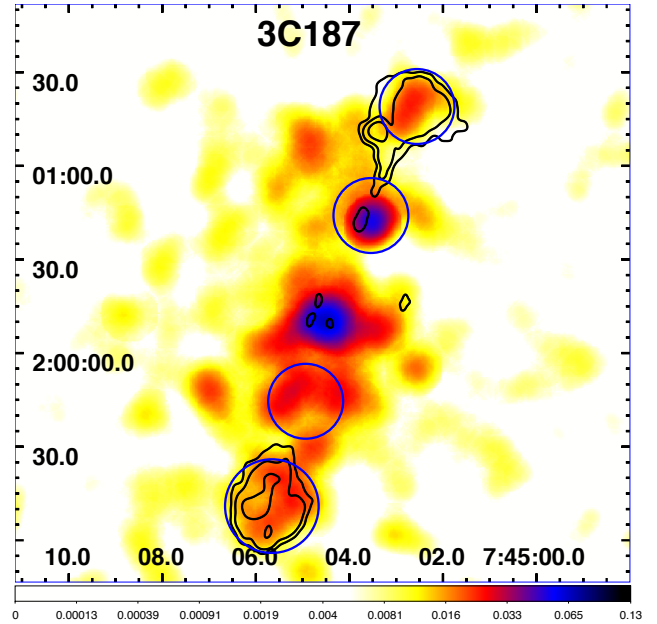


FIG. 2.— 3C 187 (0.5-7 keV) smoothed with a Gaussian of FWHM= $11''$. The color bar gives the brightness in units of counts/pixel and the pixel size is $0.492''$. The four regions listed in Table 3 are shown in blue. The contours come from an L band radio map with a clean beam of $3''$ and start at 1 mJy/beam, increasing by factors of 4.

3C 268.2 is an FR II radio galaxy with no nuclear radio emission detectable in the 1.4 GHz map available to us. An X-ray source lies between the radio emission arising from the hotspot regions so is plausibly the X-ray core. The X-ray nucleus is elongated in the EW direction. In the HST image the source has strong extended emission-line regions which could be responsible for its apparent elongated morphology (de Koff et al. 1996). In addition, a marginal detection of the X-ray counterpart of the southern hotspot has been found.

3C 274.1 is an FR II radio galaxy that lies in a galaxy cluster (Yates et al. 1989). At this position, we find cluster #95983 in the list compiled by Wen et al. (2012), based on the Sloan Digital Sky Survey. However, in the X-rays, only the nucleus (that appears to be extended) is detected.

3C 275 is an FR II radio galaxy optically classified as LEG. In all the radio maps available to us ranging from 1.4 GHz up to 14.9 GHz, the radio nucleus is not detected, thus the alignment between X-ray and radio emissions is not precise, since the maps have not been registered. The extended X-ray emission arising from the core of 3C 275 was clearly detected. The original optical identification (Kristian et al. 1974) reports the galaxy is in a distant cluster but we have no direct evidence for that.

3C 306.1 is a radio galaxy optically classified as HEG and radio classified as FR II. In the *Chandra* observation, the X-ray nucleus, which is not point-like, was seen. 3C 306.1 is also a member of a galaxy cluster (Yates et al. 1989) but its X-ray thermal emission was not seen in the 3C snapshot survey.

3C 313 is an FR II radio galaxy optically classified as an HEG. The galaxy nucleus is surrounded by patches of optical emission in the HST images (de Koff et al. 1996).

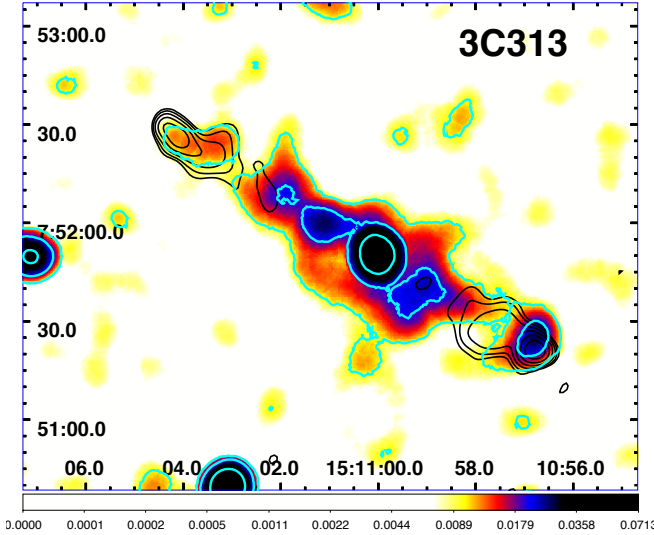


FIG. 3.— An X-ray image of 3C 313 for the energy band 0.5–7 keV. The pixel size is $0.492''$ and the smoothing function is a Gaussian of $\text{FWHM}=11.0''$. X-ray contours (white or cyan) start at 0.01 counts/pix and increase by factors of two. The radio contours (black) come from a 1.4 GHz map constructed from archival VLA data and start at 15 mJy/beam, increasing by factors of two. The clean beam is $5''$.

Although no clear signatures of X-ray cluster emission was found, 3C 313 is a member of a galaxy cluster (Hill & Lilly 1991; Stanford et al. 2002). At this position, we find cluster #107171 in the list compiled by Wen et al. (2012), based on the Sloan Digital Sky Survey. There is, however enhanced X-ray brightness along the entire principle axis of the radio source; i.e. even close to the nucleus where no radio emission is seen with the data available to us (VLA, 1.4 GHz and 8.4 GHz) (see Figure 3). In addition to this extended emission which could be either thermal (e.g., extended optical emission line region) or non-thermal (e.g., inverse Compton emission from radio emitting electrons scattering CMB photons), 4 counts were detected near the tip of the northern hotspot and 9 counts are aligned with the southern hotspot.

3C 320 is a classical FR II radio galaxy located in the center of a cluster of galaxies (Spinrad et al. 1985). At this position, we find cluster #115229 in the list compiled by Wen et al. (2012), based on the Sloan Digital Sky Survey. 3C 320 shares many attributes with Cygnus A. The eastern hotspot/lobe has engendered an obvious cavity in the cluster gas. In the *Chandra* observations of 12ksec, 1046 ± 37 net counts were found in the 0.5 – 7 keV energy range within a circular region of $1'$ radius (286 kpc).

3C 327.1 is optically classified as HEG hosted in a normal elliptical galaxy (de Koff et al. 1996). This radio source has a curved jet on the SE side, and only a low brightness lobe to the NW. Its radio structure (Morganti et al. 1999) is remarkably similar to that of the low redshift radio source 3C 17 (Massaro et al. 2009). The X-ray emission is extended around the nucleus and a trace of the southern jet can be seen in the X-ray image (see Figure in Appendix B).

3C 341 is a classical FR II radio galaxy optically classified as HEG. High resolution radio maps at 8 GHz show a

slightly curved line of enhanced brightness over the first half of the SW lobe. At $\approx 8''$ from the nucleus there is a knot ≈ 4 times brighter than adjoining areas. At the position of this knot in the jet there are 2.5 ± 1.8 net X-ray counts.

3C 411 is an FR II radio galaxy with high excitation emission lines in its optical spectrum. The X-ray core is the brightest detected in the current sample with ≈ 0.75 counts/frame and is thus affected by substantial pileup. The ratio of evt1 counts to evt2 counts is 1.26.

3C 434 is an FR II radio galaxy hosted in an elliptical galaxy, whose optical emission is slightly elongated in the southeast direction (de Koff et al. 1996). This radio galaxy lies close to a galaxy group according to Yates et al. (1989), however, the X-ray snapshot observation only revealed nuclear emission.

3C 435 is comprised of two double-lobed radio galaxies. 3C 435A is an FR II radio galaxy at redshift 0.471 (Spinrad et al. 1985) and 3C 435B is another FR II radio source lying $10''$ away but at $z=0.865$ (McCarthy et al. 1989). The X-ray core of 3C 435A is undetected in the *Chandra* snapshot observation, while X-ray emission was detected from the nuclear region of 3C 435B. It is worth noting that a blue stellar object (A type star) lies in the direction of 3C 435B (McCarthy et al. 1989), however given the significant X-ray emission above ~ 2 keV, we suspect the *Chandra* detection arises from the host galaxy of 3C 435B.

4. SUMMARY

We have presented the X-ray analyses of 19 3C radio sources with redshift between 0.3 and 0.5. Since proprietary rights were waived, X-ray data based on a radio flux limited sample (almost all extragalactic 3C sources with $z < 0.5$) are now available to the community. The main objectives of this 3C snapshot survey are: to detect X-ray emission from jets and hotspots, and to study the nuclear emission of their host galaxies. In the present work, the basic source parameters for the newly acquired data are presented, while in future works, the resulting datasets will be used to test several issues such as the Fanaroff-Riley dichotomy and differences in the nature of nuclear absorption in FRI and FR II sources.

Fluxmaps for all the X-ray observations were constructed and we provide photometric results for the nuclei and other radio structures (i.e., jet knots, hotspots, lobes). Using hardness ratios, we have estimated the column density for intrinsic absorption for 16 nuclei (2 nuclei are affected by pileup and one has too few counts). In addition, for the 4 brightest nuclei, X-ray spectral analysis was performed, comparing the results on the intrinsic absorption with those derived from the hardness ratio analysis (see § 2.4).

X-ray emission was detected for all the nuclei except 3C 435A. A sizable fraction ($\sim 60\%$) of them show evidence for significant intrinsic absorption (§ 2.3 and § 2.4). Amongst these 3C *Chandra* observations, we found X-ray emission arising from one compact steep spectrum radio sources: 3C 67 and X-ray emission from two galaxy clusters surrounding 3C 19 and 3C 320. In addition, we find X-ray emission from six radio hotspots (in the four radio galaxies 3C 16, 3C 19, 3C 268.2 and 3C 313) and several knots in the radio jets of 3C 327.1 and 3C 341. Finally, in the FR II radio galaxies 3C 187 and 3C 313 extended

X-ray emission, of still unknown nature, was discovered, arising from regions along the principle radio axis (see § 3.2 for more details) .

We thank the anonymous referee for useful comments that led to improvements in the paper. We are grateful to R. Morganti, M. Hardcastle and C. C. Cheung for providing several radio maps of the 3C sources and for helpful discussions. This research has made use of NASA’s Astrophysics Data System. TOPCAT⁸ (Taylor 2005) and SAOImage DS9 were used extensively in this work for the preparation and manipulation of the tabular data and the images. SAOImage DS9 was developed by the Smithsonian Astrophysical Observatory. The NASA/IPAC Extragalactic Database (NED) is provided by the Jet Propulsion Laboratory, California Institute of Technology, under contract with

the National Aeronautics and Space Administration. Several radio maps were downloaded from the NVAS (NRAO VLA Archive Survey) and from the DRAGN webpage⁹. The National Radio Astronomy Observatory is operated by Associated Universities, Inc., under contract with the National Science Foundation. The work at SAO is supported by NASA-GRANTS GO1-12125A and GO2-13115X. This work was also supported by contributions of European Union, Valle DAosta Region and the Italian Minister for Work and Welfare. AB acknowledges support by the research group FOR 1254 funded by the Deutsche Forschungsgemeinschaft: ‘Magnetization of interstellar and intergalactic media: the prospect of low-frequency radio observations. G.R.T acknowledges support by the European Community’s Seventh Framework Programme (/FP7/2007- 2013/) under grant agreement No. 229517.

Facilities: VLA, CXO (ACIS)

REFERENCES

- Aldcroft, T. L., Siemiginowska, A., Elvis, M., Mathur, S., Nicastro, F., Murray, S. S. 2003 *ApJ*, 597, 751
- Arnaud, K.A., 1996, “Astronomical Data Analysis Software and Systems V”, eds. Jacoby G. and Barnes J., p17, ASP Conf. Series volume 101
- Balmaverde, B. et al. 2012 *A&A*, 545A, 143
- Becker, R. H., White, R. L., Helfand, D. J. 1995 *ApJ*, 450, 559
- Belsole, E., Worrall, D. M., Hardcastle, M. J. 2006 *MNRAS*, 366, 339
- Best, P. N. Rottgering H. J. A. & Lehnert, M. D. 1999 *MNRAS*, 310, 223
- Blanton, E. L., Sarazin, C. L., McNamara, B. R., Wise, M. W. 2001 *ApJ*, 558L, 15
- Blundell, K. M. & Fabian, A. C. 2011 *MNRAS*, 412, 705
- Bogdan, A. et al. 2011 *ApJ*, 743, 59
- Bondi, M., Brunetti, G., Comastri, A., & Setti, G. 2004, *MNRAS*, 354, L43
- Brinkman, A. C. et al. 2002 *A&A*, 396, 761
- Brunetti, G., Bondi, M., Comastri, A., Pedani, M., Varano, S., Setti, G., Hardcastle, M. J. 2001 *ApJ*, 561L, 157
- Brunetti, G., Bondi, M., Comastri, A., Setti, G. 2002 *A&A*, 381, 795
- Buttiglione, S., Capetti, A., Celotti, A., Axon, D.J., Chiaberge, M., Macchetto, F.D., Sparks, W.B., 2009 *A&A* 495, 1033
- Capetti, A. Macchetto, F. D., Lattanzi, M. G. 1997 *ApJ*, 476L, 67
- Carilli, C. L. 2003 *NewAR*, 47, 231
- Comastri, A., Brunetti, G., Dallacasa, D., Bondi, M., Pedani, M., Setti, G. 2003 *MNRAS*, 340L, 52
- Chiaberge, M., Capetti, A., Celotti, A. 2000 *A&A*, 355, 873
- Chiaberge, M., Gilli, R., Macchetto, F.D., Sparks, W.B., & Capetti, A. 2003 *ApJ*, 582, 645
- Condon, J. J. et al. 1998 *AJ*, 115, 1693
- Crawford, C.S., & Fabian, A.C. 2003, *MNRAS*, 339, 1163
- Davis, J. E. 2001 *ApJ*, 562, 575
- de Koff, S. et al. 1996 *ApJS*, 107, 621
- Djorgovski, S. et al. 1988 *AJ*, 96, 836
- Douglas, J. N. 1996 *AJ*, 111, 1945
- Donahue, M., Daly, R.A., & Horner, D.J. 2003, *ApJ*, 584, 643
- Donato, D., Sambruna, R. M., Gliozzi, M. 2004 *ApJ*, 617, 915
- Dunkley, J., et al. 2009 *ApJS*, 180, 306
- Edge, D. O., Shakeshaft, J. R., McAdam, W. B., Baldwin, J. E.; Archer, S. 1959 *MmRAS*, 68, 37
- Erlund, M. C.; Fabian, A. C.; Blundell, Katherine M.; Celotti, A.; Crawford, C. S. 2006 *MNRAS*, 371, 29
- Evans, D.A., Hardcastle, M.J., Croston, J.H., Worrall, D.M., & Birkinshaw, M. 2005, *MNRAS*, 359, 363
- Evans, D. A., Worrall, D. M., Hardcastle, M. J., Kraft, R. P., Birkinshaw, M. 2006 *ApJ*, 642, 96
- Evans, I. N. et al. 2010a *ApJS*, 189, 37
- Evans, D. A., Reeves, J. N., Hardcastle, M. J., Kraft, R. P., Lee, J. C., Virani, S. N. 2010b *ApJ*, 710, 859
- Fabian, A. C., Crawford, C. S., Ettori, S., Sanders, J. S. 2001 *MNRAS*, 322L, 11
- Fabian, A. C., Celotti, A., Blundell, K. M., Kassim, N. E., Perley, R. A. 2002 *MNRAS*, 331, 369
- Fabian, A. C., Celotti, A., Johnstone, R. M. 2003 *MNRAS*, 338L, 7
- Fanaroff, B. L. & Riley J. M. 1974, *MNRAS*, 167, P31
- Fernini, I., Burns, J. O., Perley R. A. 1997 *AJ*, 114, 229
- Fey, A. L. et al. 2004 *AJ*, 127, 358
- Fomalont, E. B., Petrov, L., MacMillan, D. S., Gordon, D. & Ma, C. 2003 *AJ*, 126, 2562
- Gilbert, G. M., Riley, J. M., Hardcastle, M. J., Croston, J. H., Pooley, G. G., & Alexander, P. 2004 *MNRAS* 351, 845
- Giovannini, G. et al. 2001 *ApJ* 552, 508
- Gliozzi, M., Sambruna, R. M., Eracleous, M., Yaqoob, T. 2007 *ApJ*, 664, 88
- Hardcastle, M. J., Birkinshaw, M., Worrall, D. M. 2001 *MNRAS*, 326, 1499
- Hardcastle, M. J. et al. 2002 *MNRAS*, 334, 182
- Hardcastle, M. J., Birkinshaw, M., Cameron, R. A., Harris, D. E., Looney, L. W., Worrall, D. M.
- Hardcastle, M. J. et al. 2004 *ApJ*, 612, 729
- Hardcastle, M.J., Worrall, D.M., Birkinshaw, M, Laing, R.A., & Bridle, A.H. 2005a *MNRAS*, 358, 843
- Hardcastle, M.J., Sakellou, I., & Worrall, D.M. 2005b, *MNRAS*, 359, 1007
- Hardcastle, M. J., Croston, J. H., Kraft, R. P. 2007 *ApJ*, 669, 893
- Hardcastle, M. J., Kraft, R. P., Worrall, D. M., Croston, J. H., Evans, D. A., Birkinshaw, M., Murray, S. S. 2007 *ApJ*, 662, 166
- Hardcastle, M. J., Evans, D. A., Croston, J. H. 2009 *MNRAS*, 396, 1929
- Harris, D.E., et al. 2000 *ApJ*, 530, L81
- Harris, D. E., Finoguenov, A., Bridle, A. H., Hardcastle, M. J., & Laing, R. A. 2002b, *ApJ*, 580, 110
- Harris, D. E. et al. 2006 *ApJ* 640, 211
- Harwood, J. J. & Hardcastle, M. J. 2012 *MNRAS*, 423, 1368
- Hill, G. J. & Lilly, S. J. 1991 *ApJ*, 367, 1
- Hiltner, P. R., & Roser, H. J. 1991 *A&A*, 244, 37
- Hodges-Kluck, E. J., Reynolds, C. S., Cheung, C. C., Miller, M. C. 2010 *ApJ*, 710, 1205
- Hogan, B. S., Lister, M. L., Kharb, P., Marshall, H. L., Cooper, N. J. 2011 *ApJ*, 730, 92
- Hudson, D. S. et al. 2006 *A&A*, 453, 433
- Isobe, N.; Tashiro, M.; Makishima, K.; Iyomoto, N.; Suzuki, M.; Murakami, M. M.; Mori, M.; Abe, K. 2002 *ApJ*, 580L, 111
- Jackson, N. et al. 2007 *MNRAS*, 376, 371
- Johnston, K. J. et al. 1995 *AJ*, 110, 880

⁸ <http://www.star.bris.ac.uk/~mbt/topcat/>

⁹ <http://www.jb.man.ac.uk/atlas/>

- Johnstone, R. M., Allen, S. W., Fabian, A. C., Sanders, J. S. 2002 MNRAS, 336, 299
- Kalberla, P.M.W., Burton, W. B., Hartmann, D., et al. 2005, A&A, 440, 775
- Kataoka, J., Edwards, P., Georganopoulos, M., Takahara, F., & Wagner, S. 2003a, A&A, 399, 91
- Kataoka, J., Leahy, J.P., Edwards, P.G., Kino, M., Takahara, F., Serino, Y., Kawai, N., & Martel, A.R. 2003b A&A, 410, 833
- Kataoka, J. et al. 2008, ApJ, 685, 839
- Kraft, R. P.; Hardcastle, M. J.; Worrall, D. M.; Murray, S. S. 2005 ApJ, 622, 149
- Krawczynski, H. 2002 ApJ, 569L, 27
- Kristian, J., Sandage, A., & Katem, B. 1974 ApJ 191, 43
- Lal, D. V., Kraft, R. P., Forman, W. R., Hardcastle, M. J., Jones, C., Nulsen, P. E. J., Evans, D. A., Croston, J. H., Lee, J. C. 2010 ApJ, 722, 1735
- Mackay, C. D. 1971, MNRAS, 154, 209
- Marshall, H. et al. 2001 ApJ, 549, L167
- Marshall, H.L., Miller, B.P., Davis, D.S., Perlman, E.S., Wise, M., Canizares, C.R., Harris, D.E., & Biretta, J.A. 2002, ApJ, 564, 683
- Marshall, H.L. et al. 2005, ApJS, 156, 13
- Massaro, F., Harris, D. E., Chiaberge M. et al. 2009b, ApJ, 696, 980
- Massaro, F. et al. 2010 ApJ, 714, 589 (Paper I)
- Massaro, F., Harris, D. E., Cheung, C. C. 2011 ApJS, 197, 24
- Massaro, F. et al. 2012 ApJS, 203, 31 (Paper II)
- Mazzotta, P., Kaastra, J. S., Paerels, F. B., Ferrigno, C., Colafrancesco, S., Mewe, R., Forman, W. R. 2002 ApJ, 567L, 37
- McCarthy, P. J., van Breugel, W., Spinrad, H. 1989 AJ, 97, 36
- Miller, B.P., & Brandt, W.N. 2009, ApJ, 695, 755
- Morganti, R., Oosterloo, T., Tadhunter, C. N. 1999 A&AS, 140, 355
- Nulsen, P. E. J., Hambrick, D. C., McNamara, B. R., Rafferty, D., Birzan, L., Wise, M. W., David, L. P. 2005 ApJ, 625L, 9
- Paris, I. et al. 2012 A&A, 548A, 66
- Pesce, J.E., Sambruna, R.M., Tavecchio, F., Maraschi, L., Cheung, C.C., Urry, C.M. & Scarpa, R. 2001 ApJL, 556, L79
- Perlman, E.S., Georganopoulos, M., May, E.M., Kazanas, D. 2010 ApJ, 708, 1
- Petrov, L., Kovalev, Y. Y., Fomalont, E. & Gordon, D. 2005 AJ, 129, 116
- Reynolds, Christopher S.; Brenneman, Laura W.; Stocke, John T. 2005 MNRAS, 357, 381
- Riley, J. M., Longair, M. S., & Gunn, J. E. 1980 MNRAS 192, 233
- Sambruna, R. M. et al. 2004 ApJ, 608, 698
- Schoenmakers, A. P., de Bruyn, A. G., Röttgering, H. J. A., van der Laan, H., Kaiser, C. R. 2000 MNRAS, 315, 371
- Shemmer O. et al. 2006 ApJ, 644, 86
- Siemiginowska, A. et al. 2005 ApJ, 632, 110
- Siemiginowska, A. et al. 2008 ApJ, 684, 811
- Smail, I. 2009 ApJ, 702L, 114
- Spinrad, H., Marr, J., Aguilar, L., Djorgovski, S. 1985 PASP, 97, 932
- Stanford, S. A. et al. ApJS 142, 153, 2002
- Stockton, A., Fu, H., Henry, J. P., Canalizo, G. 2006 ApJ, 638, 635
- Sun, M., Jerius, D., Jones, C. 2005 ApJ, 633, 165
- Sun, M. 2009 ApJ, 704, 1586
- Taylor, G. B., Govoni, F. Allen S. W. & Fabian, A. C. 2001 MNRAS, 326, 2
- Taylor, M. B. 2005, ASP Conf. Ser., 347, 29
- Tremblay G. R. et al. 2009 ApJS, 183, 278
- Wen, Z. L., Han, J. L., & Liu, F. S. 2012 ApJS 199, 34
- White, R. L., Becker, R. H. Helfand, D. J., Gregg, M. D. et al. 1997 ApJ, 475, 479
- Wilkes, B. J. et al. 2013 ApJ submitted
- Wilson, A.S., Young, A.J., & Shopbell, P.L. 2000 ApJL, 544, L27
- Worrall, D. M., Birkinshaw, M., Hardcastle, M. J., Lawrence, C. R. 2001 MNRAS, 326, 1127
- Worrall, D. M. 2009 A&ARv, 17, 1
- Yates, M. G., Miller, L., Peacock, J. A. 1989 MNRAS, 240, 129

APPENDIX

A. CHANDRA OBSERVATIONS OF THE 3CR SAMPLE

In Table A we list the summary of the *Chandra* observations for the whole 3CR sample. We report the 3CR name together with an alternate name for the most observed sources, the radio classification, the coordinates, the redshift (if known), the number of *Chandra* observations as well as the reference for the first *Chandra* image and some X-rays notes. In particular, we marked 3CR sources that lie in a galaxy cluster (cl) and if the cluster is also detected in the X-rays (xcl), and/or if a jet knot, hotspot, lobe is also detected in the X-rays (k,h,l, respectively) as reported in the literature. The radio classification is based on the Spinrad et al. (1985) version of the 3CR catalog, however we distinguished between FR I and FR II radio galaxies (e.g., Fanaroff & Riley 1974). Uncertain classification are labeled as “UND” while uncertain or unknown redshift estimates are marked with “?”. If the 3CR source is not observed by *Chandra* we simply reported a dashed line “-”; when no reference are listed but the number of *Chandra* observations is greater than 1 implies that the X-ray observations have not been performed or not yet been published. The absence of one or more codes in the X-ray notes does not necessarily mean there is no detection of extended emission.

References for the radio positions used in Table A are: Becker et al. (1995), Best et al. (1999), Condon et al. (1998), Djorgovski et al. (1988), Douglas et al. (1996), Evans et al. (2010a), Fernini et al. (1997), Fey et al. (2004), Fomalont et al. (2003), Hiltner & Roser (1991), Jackson et al. (2007), Johnston et al. (1995), Paris et al. (2012), Petrov et al. (2005), Taylor et al. (2001), White et al. (1997).

B. IMAGES OF THE SOURCES

Although for many radio sources analyzed the X-ray data are comprised of rather few counts, the radio morphologies are shown here via contour diagrams which are superposed on X-ray event files that have been smoothed with a Gaussian. The full width half maximum (FWHM) of the Gaussian smoothing function is given in the figure captions. When there is sufficient signal to noise ratio (S/N) of the X-ray image to provide spatial information, contours were added (cyan or white) which are normally separated by factors of two. Most of the overlaid radio contours increase by factors of four. The X-ray event files shown are in units of counts/pixel in the 0.5-7 keV energy range. The primary reason figures appear so different from each other is the wide range in angular size of the radio sources.

3CR name	Other name	Class	R.A. (J2000)	Dec. (J2000)	z	Chandra obs.	Reference	X-ray notes
2	-	QSR	00 06 22.588	-00 04 24.69	1.038	1	Shemmer et al. (2006)	-
6.1	-	FR II	00 16 31.070	+79 16 49.99	0.84	2	Hardcastle et al. (2004)	h
9	-	QSR	00 20 25.219	+15 40 54.59	2.009	1	Fabian et al. (2003)	k
11.1	-	UND	00 29 44.808	+63 58 42.81	?	-	-	-
13	-	FR II	00 34 14.556	+39 24 16.65	1.351	1	Wilkes et al. (2013)	-
14	-	QSR	00 36 06.447	+18 37 59.23	1.469	1	Wilkes et al. (2013)	-
14.1	-	UND	00 36 27.12	+59 46 30.00	?	-	-	-
15	-	FR I	00 37 04.114	-01 09 08.46	0.074	1	Kataoka et al. (2003a)	k,l
16	-	FR II	00 37 45.40	+13 20 09.2	0.405	1	this work	h,l
17	-	QSR	00 38 20.528	-02 07 40.49	0.2197	1	Massaro et al. (2009a)	k
18	-	FR II	00 40 50.553	+10 03 26.78	0.188	1	Massaro et al. (2010)	-
19	-	FR II	00 40 55.044	+33 10 08.02	0.482	1	this work	cl,h
20	-	FR II	00 43 09.177	+52 03 36.05	0.174	1	Massaro et al. (2010)	-
21.1	-	UND	00 44 41.299	+66 18 42.31	?	-	-	-
22	-	FR II	00 50 56.301	+51 12 03.01	0.936	1	-	-
27	-	UNC	00 56 01.058	+68 22 30.42	0.184	-	-	-
28	-	FR I	00 55 50.58	+26 24 36.6	0.1952	5	Donato et al. (2004)	xcl
29	-	FR I	00 57 34.895	-01 23 27.37	0.0448	1	Massaro et al. (2012)	cl,k
31	NGC 383	FR I	01 07 24.959	+32 24 45.21	0.017	1	Hardcastle et al. (2002a)	cl,k
33	-	FR II	01 08 52.858	+13 20 14.20	0.0059	1	Evans et al. (2010b)	h
33.1	-	FR II	01 09 44.237	+73 11 57.10	0.181	2	Massaro et al. (2010)	-
33.2	-	UND	01 08 34.060	+69 22 33.80	?	-	-	-
34	-	FR II	01 10 18.666	+31 47 20.47	0.69	-	-	-
35	-	FR II	01 12 02.236	+49 28 35.03	0.067	1	-	-
36	-	QSR	01 17 59.480	+45 36 21.75	1.301	-	-	-
40	ARP 308	FR II	01 25 53.50	-01 21 54.00	0.018	2	Bogdan et al. (2011)	xcl
41	-	FR II	01 26 44.389	+33 13 11.21	0.795	-	-	-
42	-	FR II	01 28 30.12	+29 03 00.8	0.395	1	this work	-
43	-	QSR	01 29 59.809	+23 38 20.28	1.459	1	Wilkes et al. (2013)	-
44	-	FR II	01 31 21.765	+06 23 40.82	0.66	-	-	cl
46	-	FR II	01 35 28.48	+37 54 05.2	0.4373	1	this work	cl
47	-	QSR	01 36 24.411	+20 57 27.44	0.425	1	Hardcastle et al. (2004)	h
48	-	QSR	01 37 41.299	+33 09 35.13	0.367	1	Siemiginowska et al. (2008)	-
49	-	FR II	01 41 09.160	+13 53 28.05	0.621	1	-	-
52	-	FR II	01 48 28.909	+53 32 28.04	0.2854	1	Massaro et al. (2010)	cl,h
54	-	FR II	01 55 30.162	+43 45 55.43	0.8274	-	-	-
55	-	FR II	01 57 10.510	+28 51 37.56	0.7348	-	-	-
61.1	-	FR II	02 22 35.571	+86 19 06.38	0.1878	1	Massaro et al. (2010)	h
63	-	FR II	02 20 54.316	-01 56 50.72	0.175	1	Massaro et al. (2012)	-
65	-	FR II	02 23 43.191	+40 00 52.45	1.176	1	Wilkes et al. (2013)	-
66A	-	BL	02 22 39.611	+43 02 07.79	?	2	-	-
66B	UGC 1841	FR I	02 23 11.411	+42 59 31.38	0.0213	1	Hardcastle et al. (2001)	cl,k
67	-	FR II	02 24 12.29	+27 50 11.5	0.310	1	this work	-
68.1	-	QSR	02 32 28.872	+34 23 46.79	1.238	1	Wilkes et al. (2013)	-
68.2	-	FR II	02 34 23.856	+31 34 17.46	1.575	1	Wilkes et al. (2013)	-
69	-	FR II	02 38 02.355	+59 11 50.00	0.458	-	-	-
71	NGC 1068	Sy	02 42 40.711	-00 00 47.81	0.0037	15	Brinkman et al. (2002)	-
75	NGC 1128	FR I	02 57 41.57	+06 01 28.8	0.0231	1	Hudson et al. (2006)	xcl
76.1	-	FR II	03 03 15.054	+16 26 18.83	0.0324	1	Massaro et al. (2010)	-
78	NGC 1218	FR I	03 08 26.223	+04 06 39.30	0.0286	2	Harwood & Hardcastle (2012)	-
79	-	FR II	03 10 00.090	+17 05 58.52	0.2559	1	Massaro et al. (2012)	cl
83.1	NGC 1265	FR I	03 18 15.664	+41 51 27.88	0.0251	1	Sun et al. (2005)	xcl,k
84	NGC 1275	FR I	03 19 48.160	+41 30 42.10	0.0175	27	Fabian et al. (2002)	xcl
86	-	FR II	03 27 19.357	+55 20 28.12	?	-	-	-
88	UGC 2478	FR I	03 27 54.194	+02 33 41.98	0.0302	4	Sun (2009)	xcl
89	-	FR I	03 34 15.574	-01 10 56.09	0.1386	1	Massaro et al. (2012)	xcl
91	-	UND	03 37 43.353	+50 45 52.83	?	-	-	-
93	-	QSR	03 43 30.008	+04 57 48.58	0.3571	-	-	-
93.1	-	UNC	03 48 46.934	+33 53 15.28	0.2430	1	Massaro et al. (2012)	cl
98	-	FR II	03 58 54.442	+10 26 03.03	0.0305	1	Hodges-Kluck et al. (2010)	-

3CR name	Other name	Class	R.A. (J2000)	Dec. (J2000)	z	<i>Chandra</i> obs.	Reference	X-ray notes
99	-	Sy	04 01 07.628	+00 36 32.91	0.426	1	-	cl
103	-	FR II	04 08 03.10	+43 00 32.70	0.330	1	this work	-
105	-	FR II	04 07 16.453	+03 42 25.80	0.089	1	Massaro et al. (2010)	k,h
107	-	FR II	04 12 22.627	-00 59 32.43	0.785	-	-	-
109	-	FR II	04 13 40.37	+11 12 13.8	0.3056	1	Hardcastle et al. (2004)	h
111	-	FR II	04 18 21.277	+38 01 35.80	0.0485	2	Hogan et al. (2011)	k,h
114	-	FR II	04 20 22.170	+17 53 55.20	0.815	-	-	-
119	-	UNC	04 32 36.502	+41 38 28.44	1.023	-	-	-
123	-	FR II	04 37 04.375	+29 40 13.81	0.2177	1	Hardcastle et al. (2001)	cl,k
124	-	UNC	04 41 59.108	+01 21 01.91	1.083	-	-	-
125	-	UND	04 46 17.857	+39 45 03.03	?	-	-	-
129	WEIN 045	FR I	04 49 09.076	+45 00 39.22	0.0208	2	Krawczynski (2002)	xcl,k
129.1	WEIN 051	FR I	04 50 06.67	+45 03 05.8	0.0222	1	Krawczynski (2002)	-
130	-	FR I	04 52 52.836	+52 04 47.09	0.1090	1	Massaro et al. (2012)	-
131	-	UND	04 53 23.328	+31 29 25.30	?	-	-	-
132	-	FR II	04 56 42.919	+22 49 23.20	0.214	1	Massaro et al. (2010)	cl
133	-	FR II	05 02 58.472	+25 16 25.31	0.2775	1	Massaro et al. (2010)	-
134	-	UND	05 04 42.19	+38 06 11.4	?	-	-	-
135	-	FR II	05 14 08.367	+00 56 32.28	0.1273	1	Massaro et al. (2010)	cl
136.1	-	FR II	05 16 03.14	+24 58 25.5	0.064	1	Balmaverde et al. (2012)	-
137	-	UND	05 19 32.422	+50 54 32.08	?	-	-	-
138	-	QSR	05 21 09.886	+16 38 22.05	0.759	1	-	-
139.2	-	FR II	05 24 27.11	+28 12 47.0	?	-	-	-
141	-	UND	05 26 44.20	+32 50 23.0	?	-	-	-
142.1	-	UNC	05 31 29.375	+06 30 24.99	0.406	-	-	-
147	-	QSR	05 42 36.137	+49 51 07.23	0.545	1	-	-
152	-	UND	06 04 28.628	+20 21 21.73	?	-	-	-
153	-	FR II	06 09 32.423	+48 04 14.64	0.2769	1	Massaro et al. (2010)	cl
154	-	QSR	06 13 50.139	+26 04 36.72	0.58	-	-	-
158	-	UND	06 21 41.063	+14 32 11.19	?	-	-	-
165	-	FR II	06 43 07.400	+23 19 03.00	0.2957	1	Massaro et al. (2010)	-
166	-	FR II	06 45 24.098	+21 21 51.30	0.2449	1	Massaro et al. (2012)	-
169.1	-	FR II	06 51 15.355	+45 09 26.22	0.633	-	-	-
171	-	FR II	06 55 14.722	+54 08 57.46	0.2384	1	Massaro et al. (2010)	k,h
172	-	FR II	07 02 08.075	+25 13 46.30	0.5191	1	-	-
173	-	QSR	07 02 17.60	+37 57 19.5	1.035	-	-	-
173.1	-	FR II	07 09 18.084	+74 49 31.89	0.2921	1	Hardcastle et al. (2004)	cl,h
175	-	QSR	07 13 02.400	+11 46 14.65	0.77	1	-	-
175.1	-	FR II	07 14 04.682	+14 36 22.00	0.92	1	-	-
180	-	FR II	07 27 04.880	-02 04 30.33	0.22	1	Massaro et al. (2012)	-
181	-	QSR	07 28 10.305	+14 37 36.24	1.382	1	Wilkes et al. (2013)	-
184	-	FR II	07 39 24.471	+70 23 10.88	0.994	1	-	xcl
184.1	-	FR II	07 43 01.394	+80 26 26.09	0.1182	1	Massaro et al. (2010)	cl
186	-	QSR	07 44 17.452	+37 53 17.15	1.067	5	Siemiginowska et al. (2005)	xcl
187	-	FR II	07 45 04.46	+02 00 08.70	0.350	1	this work	l
190	-	QSR	08 01 33.559	+14 14 42.94	1.1944	1	Wilkes et al. (2013)	-
191	0802+103	QSR	08 04 47.972	+10 15 23.69	1.956	2	Sambruna et al. (2004)	l
192	-	FR II	08 05 34.996	+24 09 50.34	0.0597	1	Hodges-Kluck et al. (2010)	cl
194	-	UNC	08 10 03.619	+42 28 04.31	1.184	-	-	-
196	-	QSR	08 13 36.033	+48 13 02.56	0.871	1	-	-
196.1	-	FR II	08 15 28.10	-03 08 28.00	0.198	1	Massaro et al. (2012)	-
197.1	-	FR II	08 21 33.605	+47 02 37.40	0.1301	1	Massaro et al. (2010)	cl
198	-	FR II	08 22 31.80	+05 57 07.90	0.0815	1	Massaro et al. (2012)	cl
200	-	FR II	08 27 25.397	+29 18 44.90	0.458	1	Hardcastle et al. (2004)	h
204	-	QSR	08 37 44.956	+65 13 34.92	1.112	1	Wilkes et al. (2013)	-
205	-	QSR	08 39 06.459	+57 54 17.12	1.534	1	Wilkes et al. (2013)	-
207	-	QSR	08 40 47.588	+13 12 23.56	0.6808	2	Brunetti et al. (2002)	h
208	-	QSR	08 53 08.609	+13 52 54.98	1.1115	1	Wilkes et al. (2013)	-
208.1	-	UNC	08 54 39.289	+14 05 52.56	1.02	-	-	-
210	-	UNC	08 58 09.961	+27 50 51.57	1.169	1	-	xcl

3CR name	Other name	Class	R.A. (J2000)	Dec. (J2000)	z	Chandra obs.	Reference	X-ray notes
212	-	QSR	08 58 41.498	+14 09 43.97	1.048	1	Aldcroft et al. (2003)	h
213.1	-	FR I	09 01 05.269	+29 01 46.88	0.1937	1	Massaro et al. (2010)	cl,h
215	-	QSR	09 06 31.873	+16 46 11.87	0.4121	1	Hardcastle et al. (2004)	-
216	-	QSR	09 09 33.497	+42 53 46.48	0.6702	1	-	-
217	-	FR II	09 08 50.583	+37 48 19.21	0.8975	-	-	-
219	-	FR II	09 21 08.623	+45 38 57.39	0.1744	1	Comastri et al. (2003)	cl,k
220.1	-	FR II	09 32 39.646	+79 06 31.53	0.61	1	Worrall et al. (2001)	xcl
220.2	-	QSR	09 30 33.473	+36 01 24.17	1.1577	-	-	-
220.3	-	FR II	09 39 22.52	+83 15 24.5	0.68	1	-	-
222	-	FR I	09 36 32.019	+04 22 10.30	1.339	-	-	-
223	-	FR II	09 39 52.755	+35 53 58.86	0.1368	1	Massaro et al. (2012)	cl
223.1	-	FR II	09 41 24.019	+39 44 41.62	0.1075	1	Massaro et al. (2010)	-
225A	-	UNC	09 42 08.480	+13 51 54.23	1.565	-	-	-
225B	-	FR II	09 42 15.387	+13 45 50.52	0.58	-	-	-
226	-	FR II	09 44 16.376	+09 46 19.25	0.8177	1	-	-
227	-	FR II	09 47 45.163	+07 25 20.34	0.0858	2	Hardcastle et al. (2007a)	h
228	-	FR II	09 50 10.791	+14 20 00.63	0.5524	2	Belsole et al. (2006)	-
230	-	UNC	09 51 58.826	-00 01 27.23	1.487	-	-	-
231	M 82	FR I	09 55 52.725	+69 40 45.78	0.00067	26	-	-
234	-	FR II	10 01 49.526	+28 47 08.87	0.1848	1	Massaro et al. (2012)	h
236	-	FR II	10 06 01.735	+34 54 10.43	0.1005	2	-	-
237	-	FR II	10 08 00.030	+07 30 16.35	0.877	-	-	-
238	-	UNC	10 11 00.379	+06 24 39.72	1.405	-	-	-
239	-	FR II	10 11 45.415	+46 28 19.75	1.781	-	-	-
241	-	FR II	10 21 54.527	+21 59 30.71	1.671	1	Wilkes et al. (2013)	-
244.1	-	FR II	10 33 33.98	+58 14 35.70	0.428	1	this work	cl
245	-	QSR	10 42 44.605	+12 03 31.26	1.0286	1	Sambruna et al. (2004)	-
247	-	FR II	10 58 58.785	+43 01 23.12	0.7489	-	-	-
249	-	QSR	11 02 03.848	-01 16 17.39	1.554	-	-	-
249.1	-	QSR	11 04 13.686	+76 58 58.02	0.3115	1	Stockton et al. (2006)	-
250	-	FR II	11 08 52.129	+25 00 54.61	?	-	-	-
252	-	FR II	11 11 32.990	+35 40 41.64	1.1	1	Wilkes et al. (2013)	-
254	-	QSR	11 14 38.736	+40 37 20.47	0.7361	1	Donahue et al. (2003)	h
255	-	QSR	11 19 25.238	-03 02 51.50	1.355	-	-	-
256	-	UNC	11 20 43.024	+23 27 55.22	1.819	1	-	-
257	-	UNC	11 23 09.172	+05 30 19.47	2.474	-	-	-
258	-	UNC	11 24 43.881	+19 19 29.50	0.165?	1	Massaro et al. (2012)	cl
263	-	QSR	11 39 57.043	+65 47 49.38	0.646	1	Hardcastle et al. (2002b)	h
263.1	-	FR II	11 43 25.084	+22 06 56.11	0.824	1	-	-
264	NGC 3862	FR I	11 45 05.009	+19 36 22.74	0.0217	1	Evans et al. (2006)	cl,k
265	-	FR II	11 45 28.991	+31 33 49.43	0.811	1	Bondi et al. (2004)	h
266	-	FR II	11 45 43.367	+49 46 08.24	1.275	1	Wilkes et al. (2013)	-
267	-	FR II	11 49 56.566	+12 47 19.07	1.14	1	Wilkes et al. (2013)	-
268.1	-	FR II	12 00 19.210	+73 00 45.70	0.97	1	-	-
268.2	-	FR II	12 00 58.61	+31 33 19.90	0.362	1	this work	h
268.3	-	FR II	12 06 24.699	+64 13 36.80	0.3717	2	-	cl
268.4	-	QSR	12 09 13.617	+43 39 20.96	1.3978	1	Wilkes et al. (2013)	-
270	NGC 4261	FR I	12 19 23.220	+05 49 30.77	0.00746	2	Chiaberge et al. (2003)	cl,k
270.1	-	QSR	12 20 33.875	+33 43 12.05	1.5324	2	Wilkes et al. (2013)	-
272	-	FR II	12 24 28.52	+42 06 36.3	0.944	-	-	-
272.1	M 84	FR I	12 25 03.743	+12 53 13.14	0.0035	4	Harris et al. (2002)	cl,k
273	-	QSR	12 29 06.699	+02 03 08.59	0.1583	27	Marshall et al. (2001)	k
274	M 87	FR I	12h30m49.423	+12 23 28.04	0.00436	110	Marshall et al. (2002)	xcl,k
274.1	-	FR II	12 35 26.66	+21 20 34.8	0.422	1	this work	-
275	-	FR II	12 42 19.89	-04 46 20.1	0.480	1	this work	cl
275.1	-	QSR	12 43 57.650	+16 22 53.54	0.5551	1	Crawford & Fabian (2003)	k,h
277	-	UNC	12 51 43.580	+50 34 24.90	0.414	-	-	-
277.1	Q1250+568	QSR	12 52 26.349	+56 34 19.66	0.3198	1	Siemiginowska et al. (2008)	-
277.2	-	FR II	12 53 33.038	+15 42 29.21	0.766	-	-	-
277.3	Coma A	FR II	12 54 12.013	+27 37 33.94	0.0853	3	-	-

3CR name	Other name	Class	R.A. (J2000)	Dec. (J2000)	z	<i>Chandra</i> obs.	Reference	X-ray notes
280	-	FR II	12 56 57.002	+47 20 19.87	0.996	1	Donahue et al. (2003)	cl,h
280.1	-	QSR	13 00 33.304	+40 09 07.72	1.6713	-	-	-
284	-	FR II	13 11 04.666	+27 28 07.15	0.2394	1	Massaro et al. (2012)	-
285	-	FR II	13 21 17.877	+42 35 15.16	0.0794	1	Hardcastle et al. (2007b)	-
286	-	QSR	13 31 08.287	+30 30 32.95	0.8493	1	-	-
287	Q1328+254	QSR	13 30 37.690	+25 09 10.87	1.055	1	Siemiginowska et al. (2008)	-
287.1	-	FR II	13 32 53.257	+02 00 45.60	0.2156	1	Massaro et al. (2010)	h
288	-	FR I	13 38 49.87	+38 51 09.2	0.246	1	Lal et al. (2010)	xcl
288.1	-	QSR	13 42 13.273	+60 21 42.85	0.9645	-	-	-
289	-	FR II	13 45 26.367	+49 46 32.59	0.9674	1	-	-
292	-	FR II	13 50 42.04	+64 29 30.6	0.71	-	-	-
293	-	FR I	13 52 17.789	+31 26 46.44	0.045	2	Massaro et al. (2010)	-
293.1	-	FR II	13 54 40.97	+16 14 50.1	0.709	-	-	-
294	-	FR II	14 06 44.022	+34 11 25.10	1.779	3	Fabian et al. (2001)	xcl,h
295	-	FR II	14 11 20.519	+52 12 09.97	0.4641	2	Harris et al. (2000)	cl,h
296	NGC 5532	FR I	14 16 52.950	+10 48 26.60	0.0247	1	Hardcastle et al. (2005a)	k
297	-	QSR	14 17 23.999	-04 00 47.54	1.4061	-	-	-
298	Q1416+067	QSR	14 19 08.180	+06 28 34.80	1.4373	2	Siemiginowska et al. (2008)	-
299	-	FR II	14 21 05.58	+41 44 48.5	0.367	2	-	cl
300	-	FR II	14 22 59.861	+19 35 36.72	0.27	1	Massaro et al. (2010)	-
300.1	-	UNC	14 28 31.314	-01 24 07.97	1.1588	-	-	-
303	-	FR I	14 43 02.780	+52 01 37.27	0.1411	1	Kataoka et al. (2003b)	cl,k,h
303.1	-	UNC	14 43 14.800	+77 07 29.00	0.267	1	Massaro et al. (2010)	-
305	-	FR II	14 49 21.661	+63 16 14.12	0.0416	2	Massaro et al. (2009b)	-
305.1	-	FR II	14 47 09.56	+76 56 21.8	1.132	-	-	-
306.1	-	FR II	14 55 01.40	-04 20 59.8	0.441	1	this work	cl
309.1	Q1458+718	QSR	14 59 07.583	+71 40 19.86	0.905	1	Siemiginowska et al. (2008)	-
310	-	FR I	15 04 57.10	+26 00 56.88	0.0538	1	Kraft et al. (2012)	xcl
313	-	FR II	15 11 00.03	+07 51 50.1	0.461	1	this work	h
314.1	-	FR I	15 10 27.064	+70 46 07.37	0.1197	1	Massaro et al. (2012)	cl
315	-	FR I	15 13 40.054	+26 07 30.06	0.1083	1	Massaro et al. (2010)	cl
317	-	FR I	15 16 44.489	+07 01 17.85	0.0344	11	Blanton et al. (2001)	xcl
318	-	FR II	15 20 05.448	+20 16 05.76	1.574	1	Wilkes et al. (2013)	-
318.1	NGC 5920	UNC	15 21 51.851	+07 42 31.75	0.0453	1	Mazzotta et al. (2002)	xcl
319	-	FR II	15 24 05.640	+54 28 18.40	0.192	1	Massaro et al. (2012)	cl
320	-	FR II	15 31 25.37	+35 33 40.0	0.342	1	this work	cl
321	-	FR II	15 31 43.512	+24 04 18.82	0.0961	2	Hardcastle et al. (2004)	h
322	-	FR II	15 35 01.230	+55 36 52.87	1.681	-	-	-
323	-	UNC	15 41 45.534	+60 15m35.07	0.679	-	-	-
323.1	-	QSR	15 47 43.545	+20 52 16.54	0.2643	1	Massaro et al. (2010)	cl
324	-	FR II	15 49 48.897	+21 25 38.06	1.2063	1	-	cl
325	-	FR II	15 49 58.424	+62 41 21.66	1.135	2	Hardcastle et al. (2009)	-
326	-	FR II	15 52 09.14	+20 05 35.8	0.0895	3	-	-
326.1	-	FR II	15 56 10.068	+20 04 20.44	1.825	-	-	-
327	-	FR II	16 02 27.375	+01 57 56.16	0.1048	1	Hardcastle et al. (2007a)	cl
327.1	-	UNC	16 04 45.38	+01 17 50.3	0.462	1	this work	k
330	-	FR II	16 09 36.607	+65 56 43.61	0.55	1	Hardcastle et al. (2002b)	cl
332	-	FR II	16 17 42.540	+32 22 34.49	0.1515	1	Massaro et al. (2010)	cl
334	-	QSR	16 20 21.819	+17 36 24.01	0.5551	1	Hardcastle et al. (2002a)	-
336	-	QSR	16 24 39.086	+23 45 12.20	0.9273	1	-	-
337	-	FR II	16 28 52.846	+44 19 05.08	0.635	1	-	cl
338	NGC 6166	FR I	16 28 38.480	+39 33 05.60	0.03035	6	Johnstone et al. (2002)	xcl
340	-	FR II	16 29 36.932	+23 20 14.42	0.7754	1	-	-
341	-	FR II	16 28 03.98	+27 41 39.3	0.448	1	this work	k
343	-	QSR	16 34 33.789	+62 45 35.81	0.988	1	-	-
343.1	-	FR II	16 38 28.193	+62 34 44.31	0.75	1	-	-
345	1641+399	QSR	16 42 58.809	+39 48 36.99	0.5928	3	Sambruna et al. (2004)	k
346	-	FR I	16 43 48.599	+17 15 49.46	0.162	1	Donato et al. (2004)	k
348	Hercules A	FR I	16 51 08.147	+04 59 33.32	0.154	3	Nulsen et al. (2005)	xcl
349	-	FR II	16 59 28.893	+47 02 55.04	0.205	1	Massaro et al. (2010)	h

3CR name	Other name	Class	R.A. (J2000)	Dec. (J2000)	z	Chandra obs.	Reference	X-ray notes
351	-	FR II	17 04 41.376	+60 44 30.50	0.3719	2	Brunetti et al. (2001)	h
352	-	FR II	17 10 44.106	+46 01 28.56	0.8067	1	-	-
353	-	FR II	17 20 28.158	-00 58 46.62	0.0304	2	Kataoka et al. (2008)	k
356	-	FR II	17 24 19.041	+50 57 40.14	1.079	1	Wilkes et al. (2013)	-
357	-	FR II	17 28 20.109	+31 46 02.58	0.1662	1	Massaro et al. (2012)	cl
368	-	FR II	18 05 06.454	+11 01 35.06	1.131	1	Wilkes et al. (2013)	-
371	-	BL	18 06 50.680	+69 49 28.10	0.051	2	Pesce et al. (2001)	k
379.1	-	FR II	18 24 32.976	+74 20 59.00	0.256	1	Massaro et al. (2012)	-
380	1828+487	QSR	18 29 31.780	+48 44 46.16	0.692	1	Marshall et al. (2005)	k
381	-	FR II	18 33 46.301	+47 27 02.61	0.1605	1	Massaro et al. (2010)	-
382	-	FR II	18 35 03.390	+32 41 46.80	0.0578	2	Glozzi et al. (2007)	-
386	-	FR I	18 38 26.255	+17 11 49.28	0.0168	1	-	-
388	-	FR II	18 44 02.40	+45 33 29.7	0.0917	2	Hodges-Kluck et al. (2010)	cl
389	-	UND	18 45 41.50	-03 07 01.92	?	-	-	-
390	-	UND	18 45 37.621	+09 53 44.71	?	-	-	-
390.3	-	FR II	18 42 08.989	+79 46 17.12	0.0561	1	Hardcastle et al. (2007a)	k,h
394	-	UND	18 59 23.362	+12 59 12.09	?	-	-	-
399.1	-	FR II	19 15 56.763	+30 19 53.79	?	-	-	-
401	-	FR II	19 40 25.117	+60 41 34.94	0.2011	2	Reynolds et al. (2005)	xcl
402	-	FR I	19 41 45.899	+50 35 45.86	0.0239	1	Massaro et al. (2012)	cl,k
403	-	FR II	19 52 15.809	+02 30 24.18	0.059	1	Kraft et al. (2005)	k,h
403.1	-	FR II	19 52 30.50	-01 17 18.00	0.0554	1	Massaro et al. (2012)	cl
405	Cygnus A	FR II	19 59 28.356	+40 44 02.09	0.056	11	Wilson et al. (2002)	xcl,h
409	-	FR II	20 14 27.596	+23 34 52.91	?	-	-	-
410	-	FR II	20 20 06.60	+29 42 14.20	0.2485	1	Massaro et al. (2012)	-
411	-	FR II	20 22 08.44	+10 01 11.30	0.467	1	this work	-
415.2	-	UND	20 32 46.115	+53 45 50.14	?	-	-	-
418	-	QSR	20 38 37.034	+51 19 12.66	1.686	-	-	-
424	-	FR I	20 48 12.087	+07 01 17.17	0.127	1	Massaro et al. (2012)	cl
427.1	-	FR II	21 04 06.865	+76 33 10.82	0.572	1	Hardcastle et al. (2004)	-
428	-	UND	21 08 22.39	+49 36 37.6	?	-	-	-
430	-	FR II	21 18 19.094	+60 48 07.77	0.0541	1	Massaro et al. (2012)	cl
431	-	UND	21 18 52.580	+49 36 58.80	?	-	-	-
432	-	QSR	21 22 46.329	+17 04 37.95	1.785	1	Erlund et al. (2006)	-
433	-	FR I	21 23 44.534	+25 04 11.88	0.1016	1	Miller & Brandt (2009)	-
434	-	FR II	21 23 16.24	+15 48 05.80	0.322	1	this work	cl
435B	-	FR II	21 29 06.10	+07 32 54.80	0.865	1	this work	-
436	-	FR II	21 44 11.743	+28 10 18.91	0.2145	2	Massaro et al. (2012)	h
437	-	FR II	21 47 25.106	+15 20 37.49	1.48	1	Wilkes et al. (2013)	-
438	-	FR II	21 55 52.290	+38 00 29.62	0.29	3	Hardcastle et al. (2004)	xcl
441	-	FR II	22 06 04.916	+29 29 19.98	0.708	1	-	-
442	-	FR I	22 14 46.90	+13 50 24.00	0.0263	4	Hardcastle et al. (20007b)	xcl
445	-	FR II	22 23 49.530	-02 06 12.85	0.0558	8	Perlman et al. (2010)	cl,h
449	-	FR I	22 31 20.9	+39 21 48.00	0.0171	3	Evans et al. (2006)	cl
452	-	FR II	22 45 48.77	+39 41 15.99	0.0811	1	Isobe et al. (2002)	h,l
454	-	QSR	22 51 34.736	+18 48 40.12	1.757	-	-	-
454.1	-	FR II	22 50 32.937	+71 29 19.18	1.841	-	-	cl
454.2	-	UND	22 52 05.41	+64 40 10.42	?	-	-	-
454.3	-	QSR	22 53 57.747	+16 08 53.56	0.859	5	Marshall et al. (2005)	k
455	-	QSR	22 55 03.889	+13 13 33.99	0.543	1	-	-
456	-	FR II	23 12 28.076	+09 19 26.39	0.2330	1	Massaro et al. (2012)	-
458	-	FR II	23 12 52.083	+05 16 49.77	0.289	1	Massaro et al. (2012)	cl,h
459	-	FR II	23 16 35.30	+04 05 18.30	0.2199	1	Massaro et al. (2012)	l
460	-	FR II	23 21 28.510	+23 46 48.45	0.268	1	Massaro et al. (2010)	cl
465	NGC 7720	FR I	23 38 29.385	+27 01 53.25	0.0302	1	Hardcastle et al. (2005b)	xcl,k
468.1	-	UND	23 50 54.849	+64 40 19.54	?	-	-	-
469.1	-	FR II	23 55 23.32	+79 55 19.60	1.336	1	Wilkes et al. (2013)	-
470	-	FR II	23 58 35.890	+44 04 45.55	1.653	1	Wilkes et al. (2013)	-

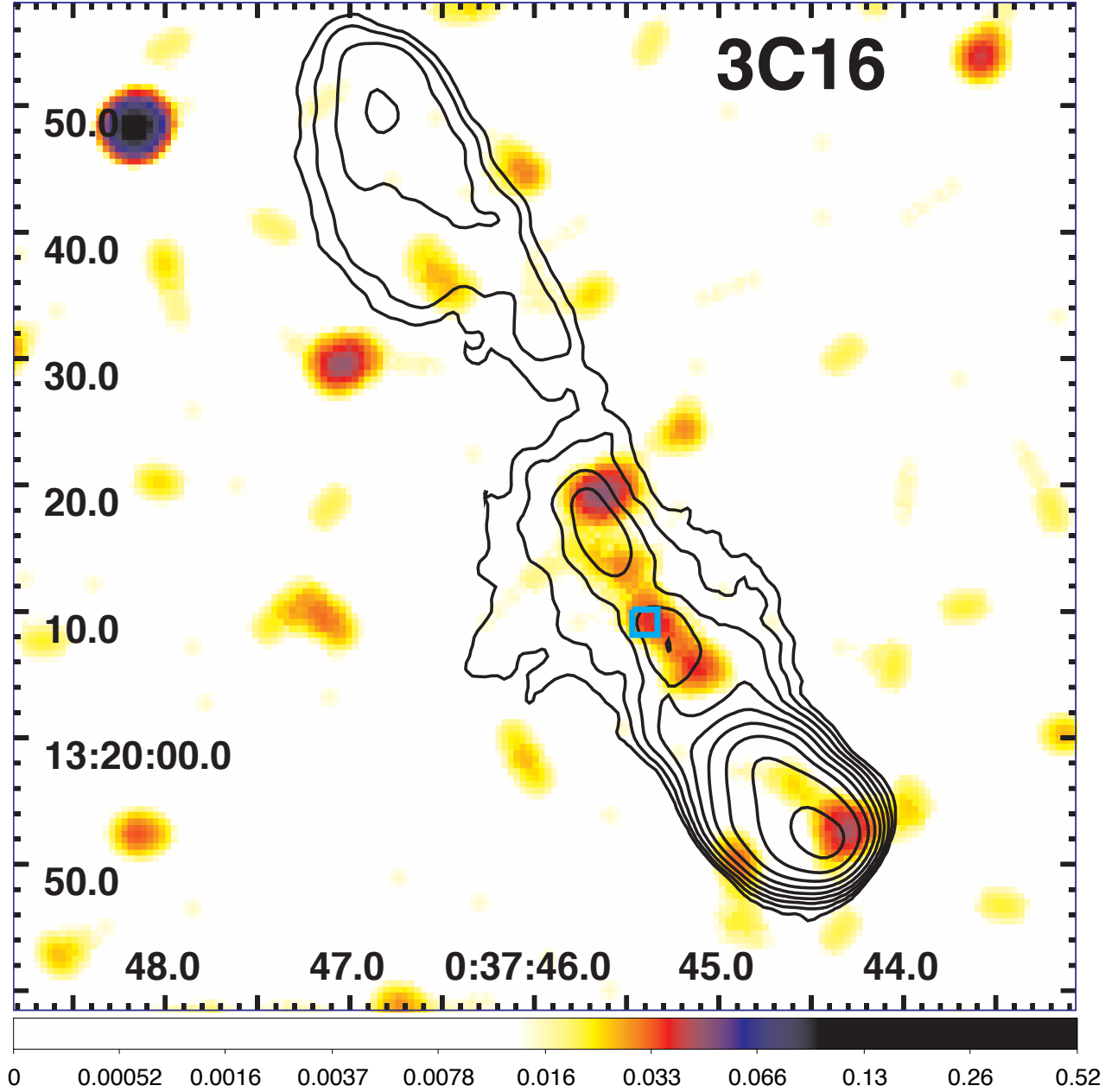


FIG. 4.— The X-ray image of 3C 16 for the energy band 0.5-7 keV. The event file has not been regridded so the pixel size is $0.492''$. The image has been smoothed with a Gaussian of $\text{FWHM}=4''$. Since there is only a marginal detection of an X-ray nucleus, the map has not been registered. The small square (cyan or black) marks the location of the optical identification: a faint galaxy with a companion (Riley et al. 1980). The radio contours (black) come from an 8.4 GHz map kindly supplied by M. J. Hardcastle (Gilbert et al. 2004) and start at 0.1 mJy/beam , increasing by factors of two. The clean beam is $2.5''$.

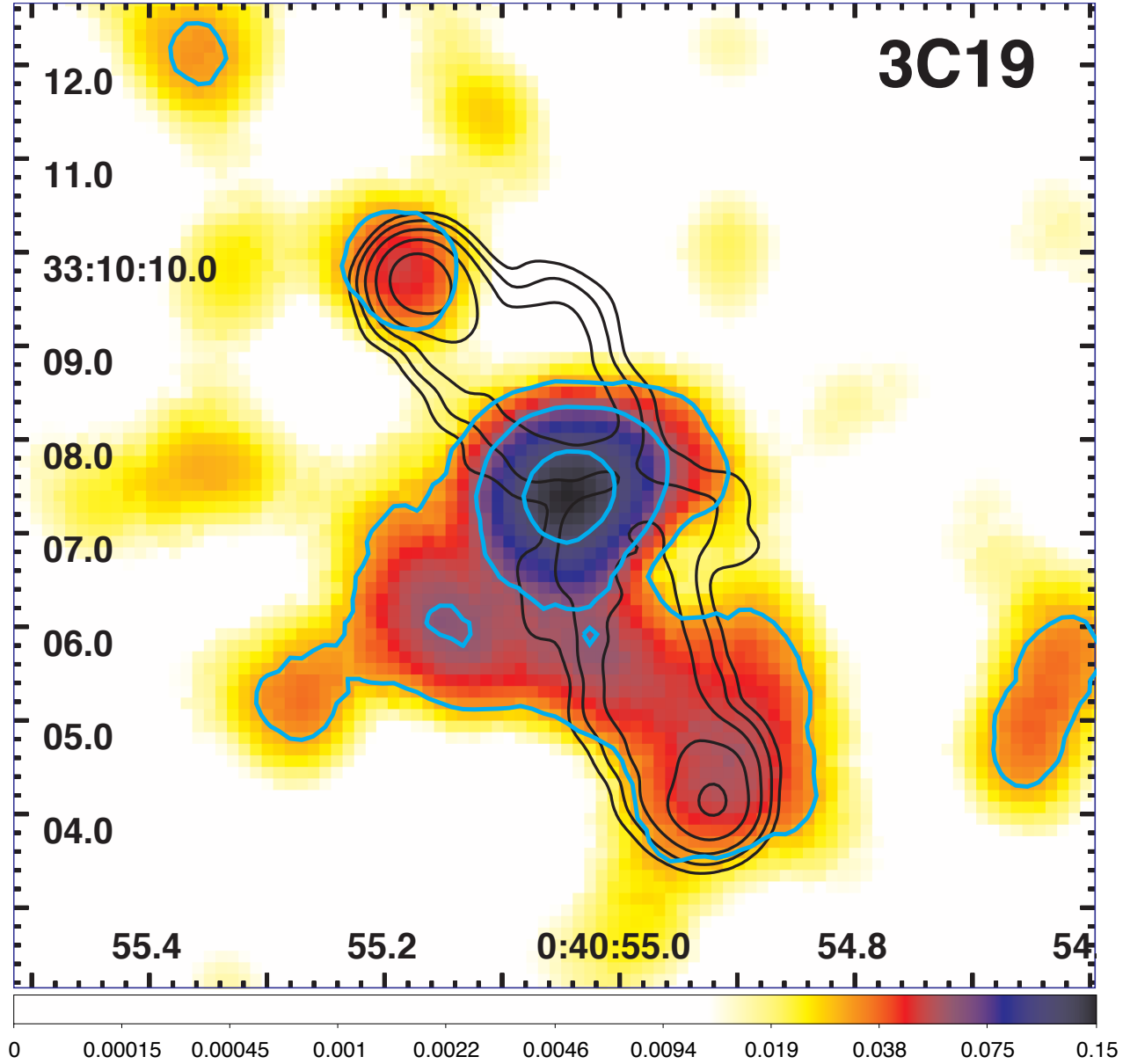


FIG. 5.— The X-ray image of 3C19 for the energy band 0.5-7 keV. The event file has been regridded to a pixel size of $0.123''$ and smoothed with a Gaussian of $\text{FWHM}=1.3''$. X-ray contours (white or cyan) start at 0.03 counts/pix and increase by factors of two. The radio contours (black) come from a 4.86 GHz map kindly supplied by M. Hardcastle (Gilbert et al. 2004) and start at 0.4 mJy/beam, increasing by factors of four. The clean beam is $0.4''$.

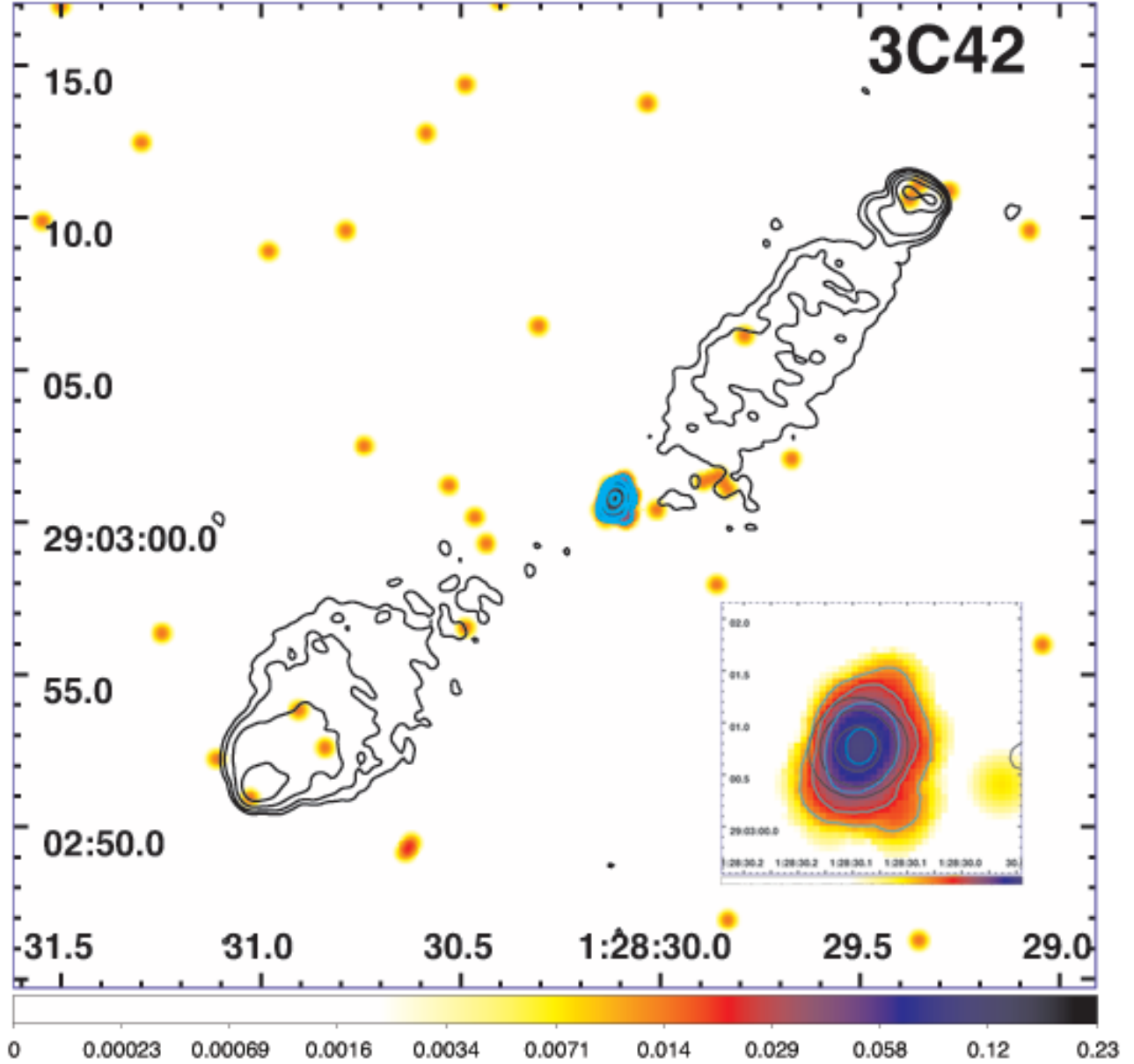


FIG. 6.— The X-ray image of 3C42 for the energy band 0.5-7 keV. The event file has been regridded to a pixel size of $0.0615''$ and smoothed with a Gaussian of $\text{FWHM}=0.5''$. X-ray contours (white or cyan) start at 0.025 counts/pix and increase by factors of two. The radio contours (black) come from an 8.4 GHz map kindly supplied by M. Hardcastle (Gilbert et al. 2004) and start at 0.1 mJy/beam, increasing by factors of four. The clean beam is $0.4''$ FWHM. The insert shows an enlarged version of the nucleus.

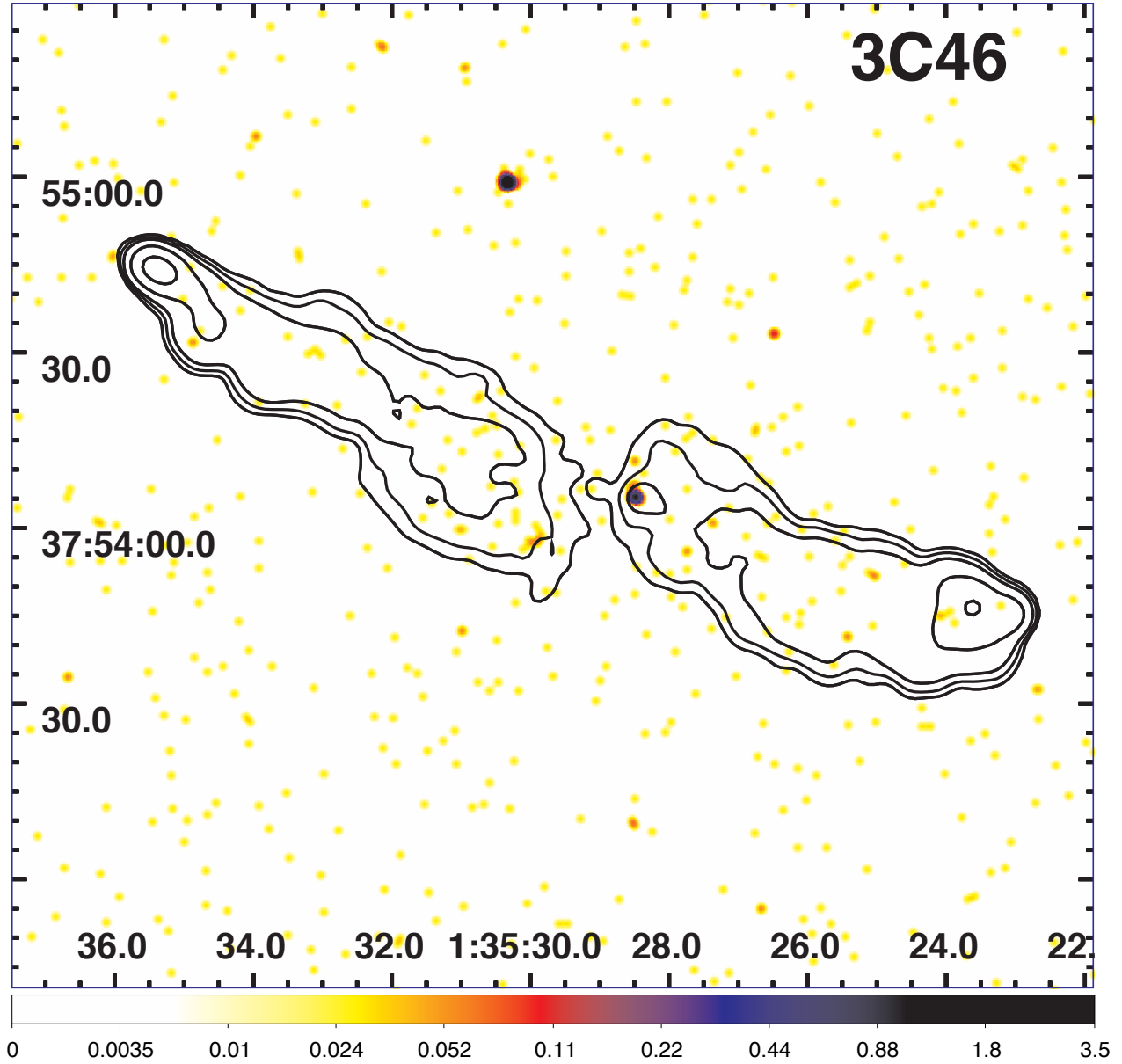


FIG. 7.— The X-ray image of 3C 46 for the energy band 0.5-7 keV. The event file has been regridded to a pixel size of $0.246''$ and smoothed with a Gaussian of $\text{FWHM}=1.45''$. The radio contours (black) come from a 1.5 GHz map from the DRAGN website and downloaded from NED. The contours start at 1 mJy/beam, increasing by factors of four (but with an extra contour at 2 mJy/beam). The clean beam is $4.2''$.

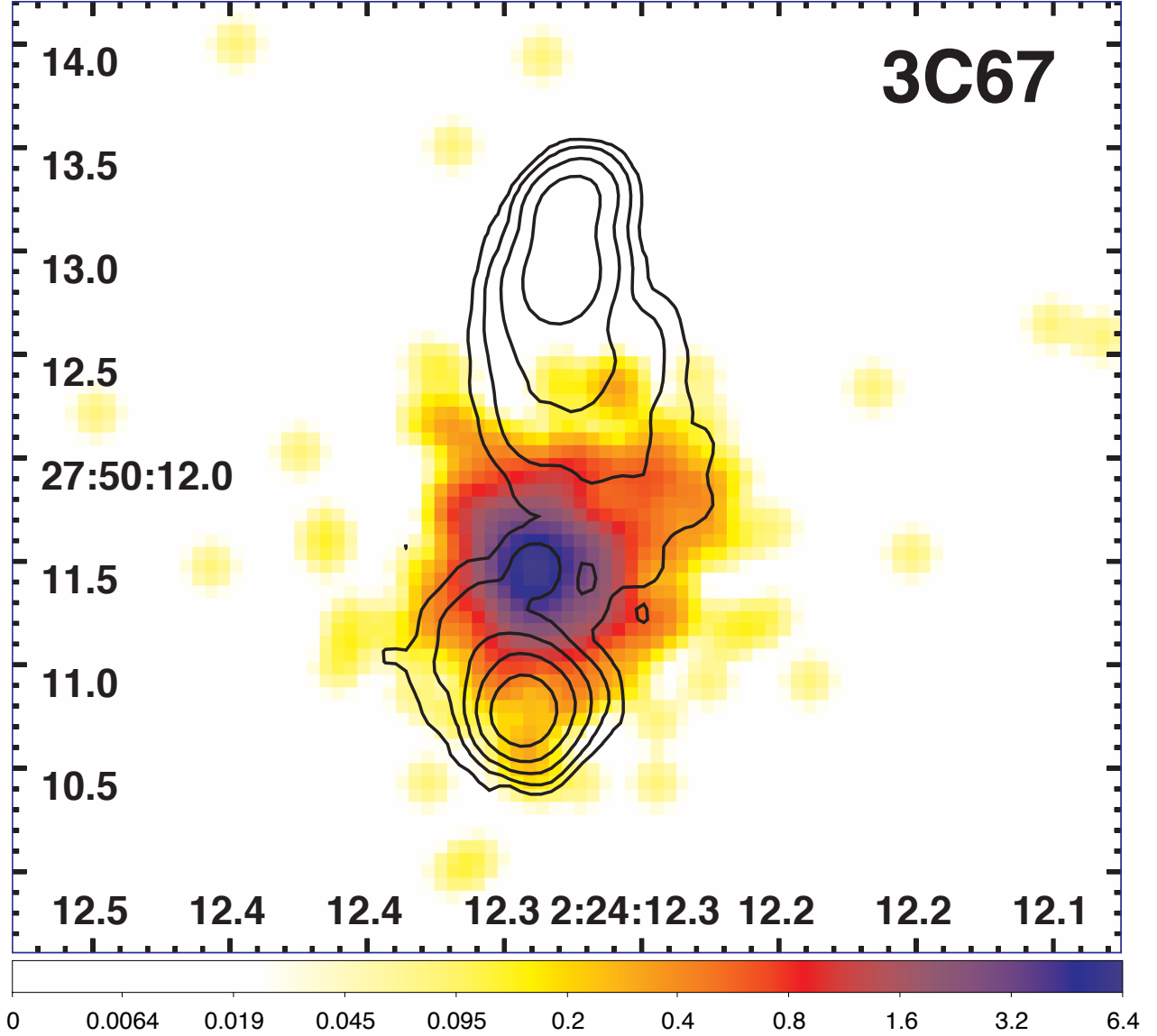


FIG. 8.— The X-ray image of 3C 67 for the energy band 0.5–7 keV. The event file has been regridded to a pixel size of $0.0615''$ and smoothed with a Gaussian of $\text{FWHM}=0.22''$. The radio contours (black) come from an 8.4 GHz VLA map kindly supplied by M. Hardcastle (Gilbert et al. 2004) and start at 0.25 mJy/beam, increasing by factors of four. The clean beam is $0.2''$.

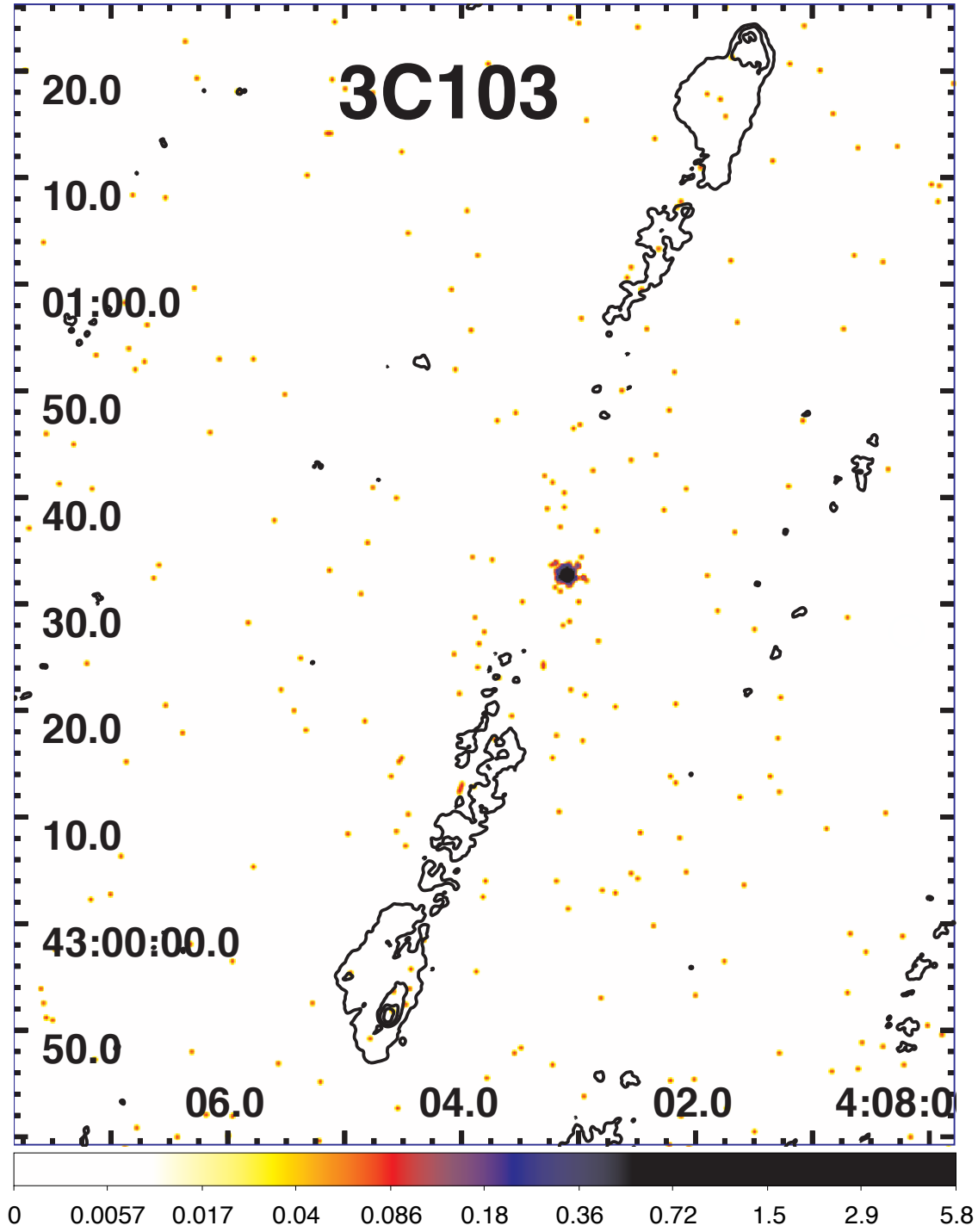


FIG. 9.— The X-ray image of 3C103 for the energy band 0.5-7 keV. The event file has been regridded to a pixel size of $0.123''$ and smoothed with a Gaussian of $\text{FWHM}=0.43''$. The radio contours (black) come from an 8.44 GHz VLA map kindly supplied by C. C. Cheung, and start at 0.3 mJy/beam, increasing by factors of four. The clean beam is $0.37''$.

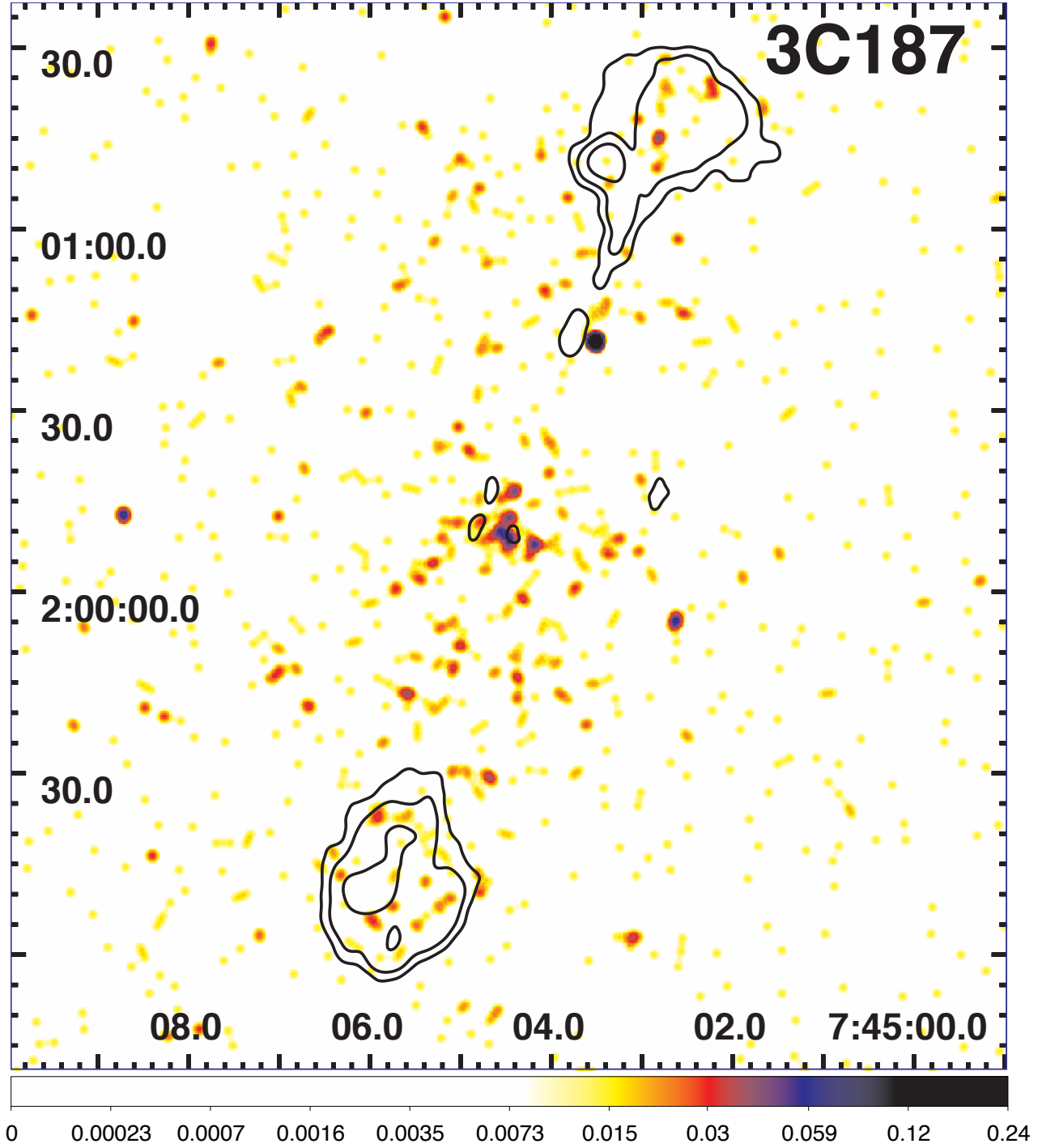


FIG. 10.— The X-ray image of 3C187 for the energy band 0.5–7 keV. The event file has been regridded to a pixel size of $0.246''$ and smoothed with a Gaussian of $\text{FWHM}=2.0''$. The radio contours (black) come from a 1.4 GHz map constructed from archival u,v data, and start at 1 mJy/beam, increasing by factors of four. The clean beam is $3.0''$. Registration of the X-ray image is approximate since there is no well defined X-ray nucleus. The VLA image at 1.4 GHz have been obtained via AIPS standard reduction procedure (<http://www.aips.nrao.edu/cook.html>).

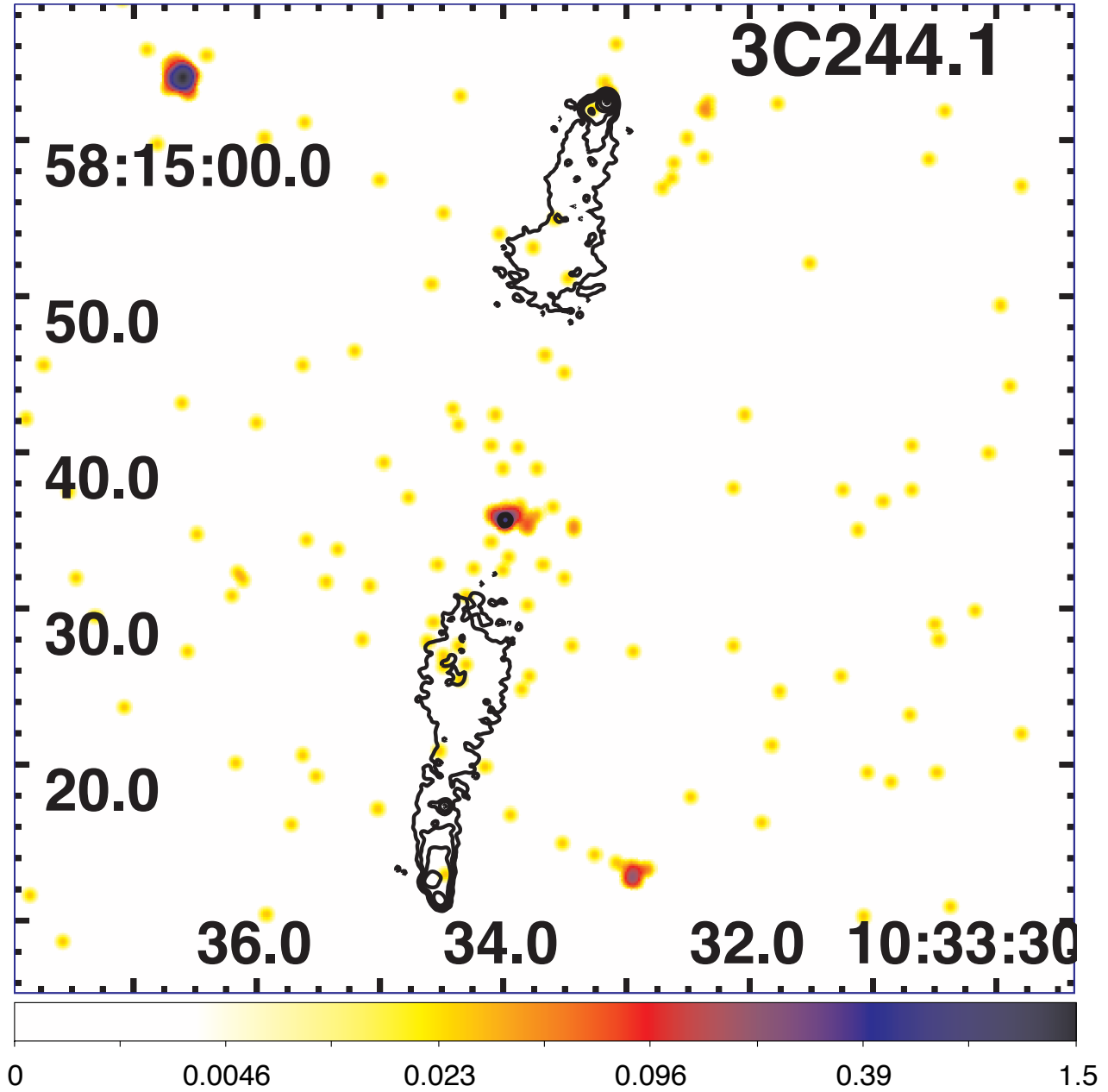


FIG. 11.— The X-ray image of 3C 244.1 for the energy band 0.5–7 keV. The event file has been regridded to a pixel size of $0.123''$ and smoothed with a Gaussian of $\text{FWHM}=0.72''$. The radio contours (black) come from a 8.45 GHz map kindly supplied by M. Hardcastle (Gilbert et al. 2004) and start at 0.1 mJy/beam, increasing by factors of four. The clean beam is $0.4''$.

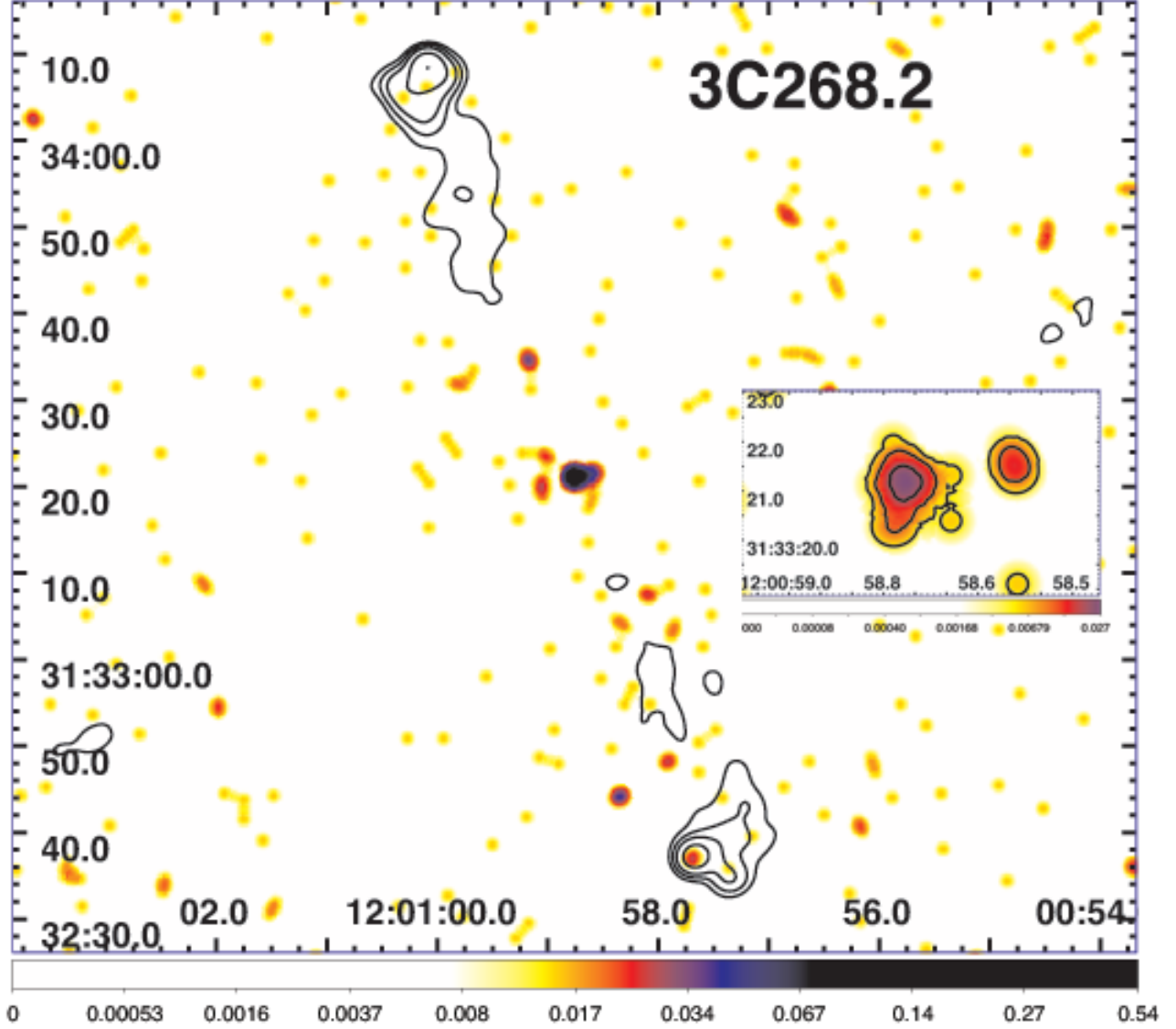


FIG. 12.— The X-ray image of 3C 268.2 for the energy band 0.5–7 keV. The event file has been regridded to a pixel size of $0.246''$ and smoothed with a Gaussian of $\text{FWHM}=2.0''$. The radio contours (black) come from a 1.4 GHz map downloaded from NED and start at 5 mJy/beam, increasing by factors of four. The clean beam is $2.7'' \times 2.5''$ with major axis in $\text{PA}=-69^\circ$. Since no radio nucleus was detected, the X-ray image has not been registered. The insert shows an enlarged version of the nuclear region. In this case, the event file has been regridded to a pixel size of $0.0615''$ and smoothed with a Gaussian of $\text{FWHM}=0.8''$. X-ray contours (white or black) are 0.005, 0.01, and 0.02 counts/pix.

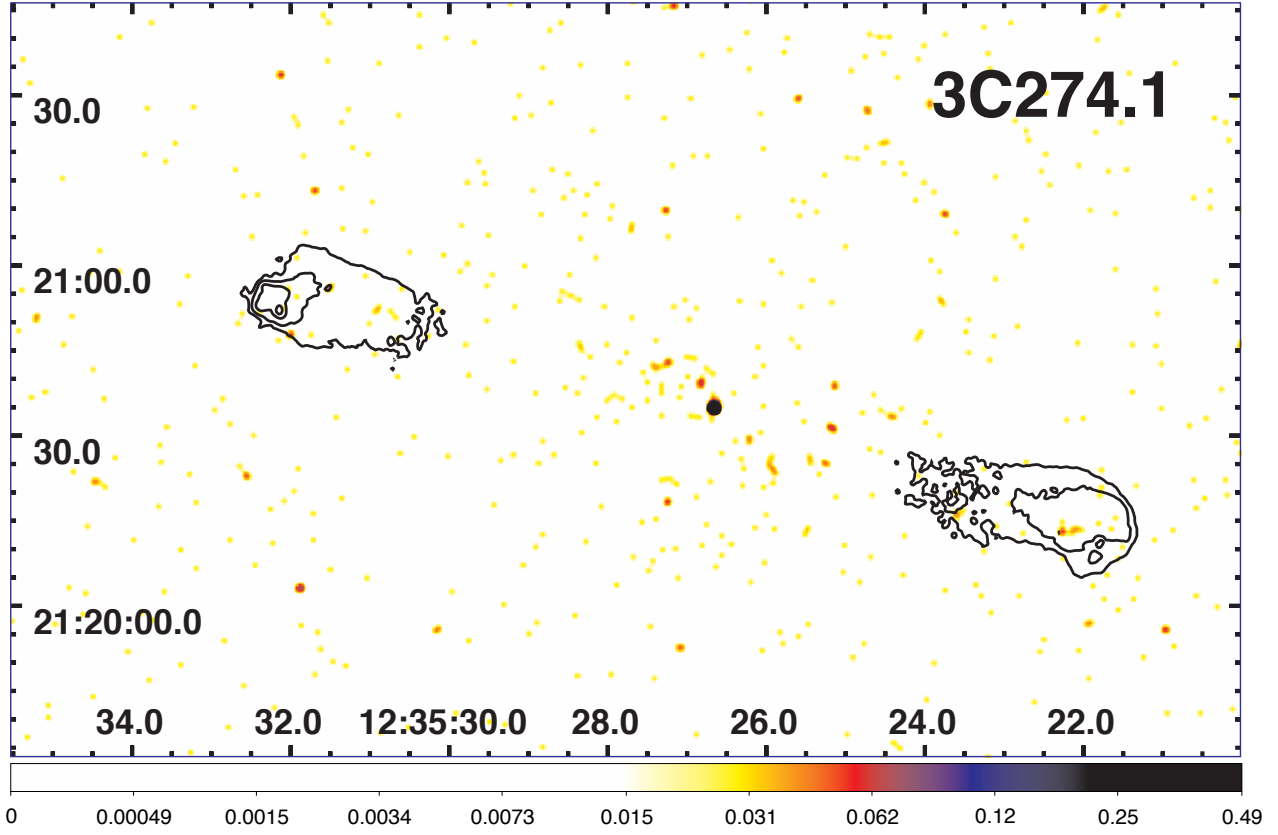


FIG. 13.— The X-ray image of 3C 274.1 for the energy band 0.5–7 keV. The event file has been regridded to a pixel size of $0.246''$ and smoothed with a Gaussian of $\text{FWHM}=1.45''$. The radio contours (black) come from an 8.5 GHz map kindly supplied by M. Hardcastle (Gilbert et al. 2004) and start at 0.125 mJy/beam, increasing by factors of four. The clean beam is $1.0''$.

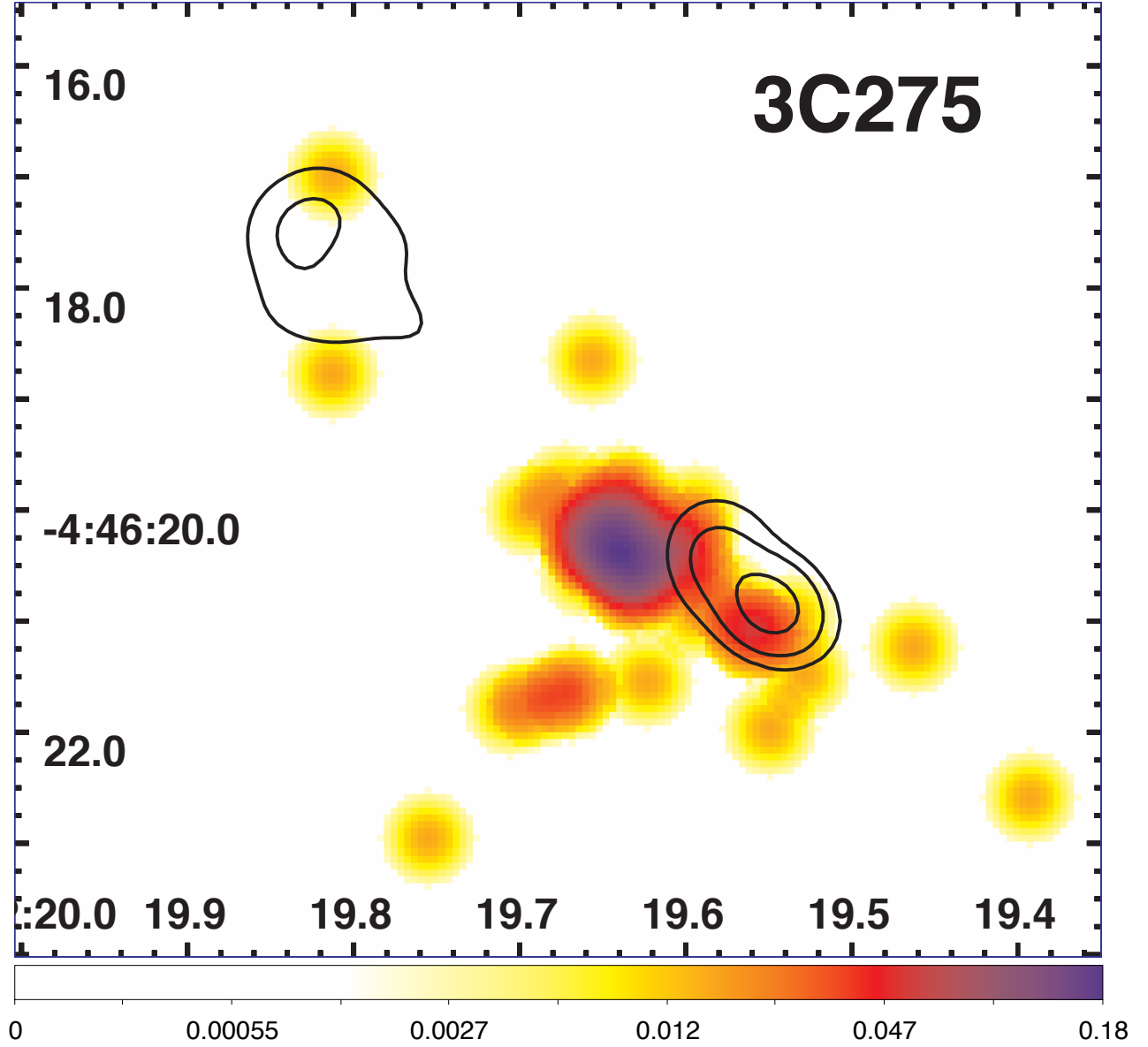


FIG. 14.— The X-ray image of 3C 275 for the energy band 0.5-7 keV. The event file has been regridded to a pixel size of $0.0615''$ and smoothed with a Gaussian of $\text{FWHM}=0.5''$. The radio contours (black) come from an 8.4 GHz map downloaded from the NVAS and start at 2 mJy/beam, increasing by factors of four. The clean beam is $0.34'' \times 0.24''$ with major axis in $\text{PA}=52^\circ$. No clear detection of the radio nucleus has been found on the maps available to us (L,C,X, and U bands); thus the X-ray map has not been registered.

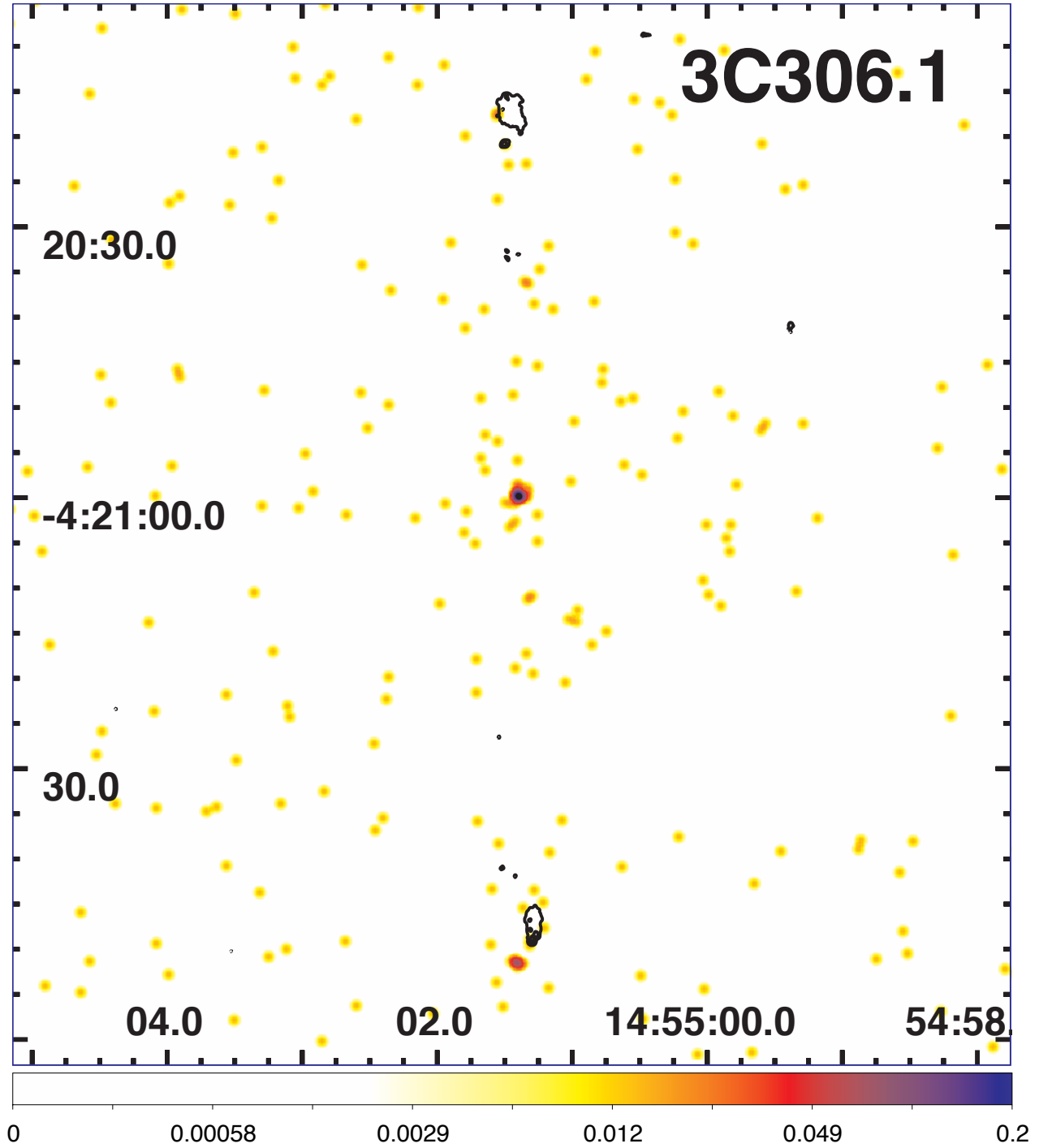


FIG. 15.— The X-ray image of 3C306.1 for the energy band 0.5–7 keV. The event file has been regridded to a pixel size of $0.123''$ and smoothed with a Gaussian of $\text{FWHM}=1''$. The radio contours (black) come from an 8.4 GHz VLA map kindly supplied by C. C. Cheung, and start at 0.5 mJy/beam, increasing by factors of four. The clean beam is $0.31''$. There are two counts aligned with the S hotspot.

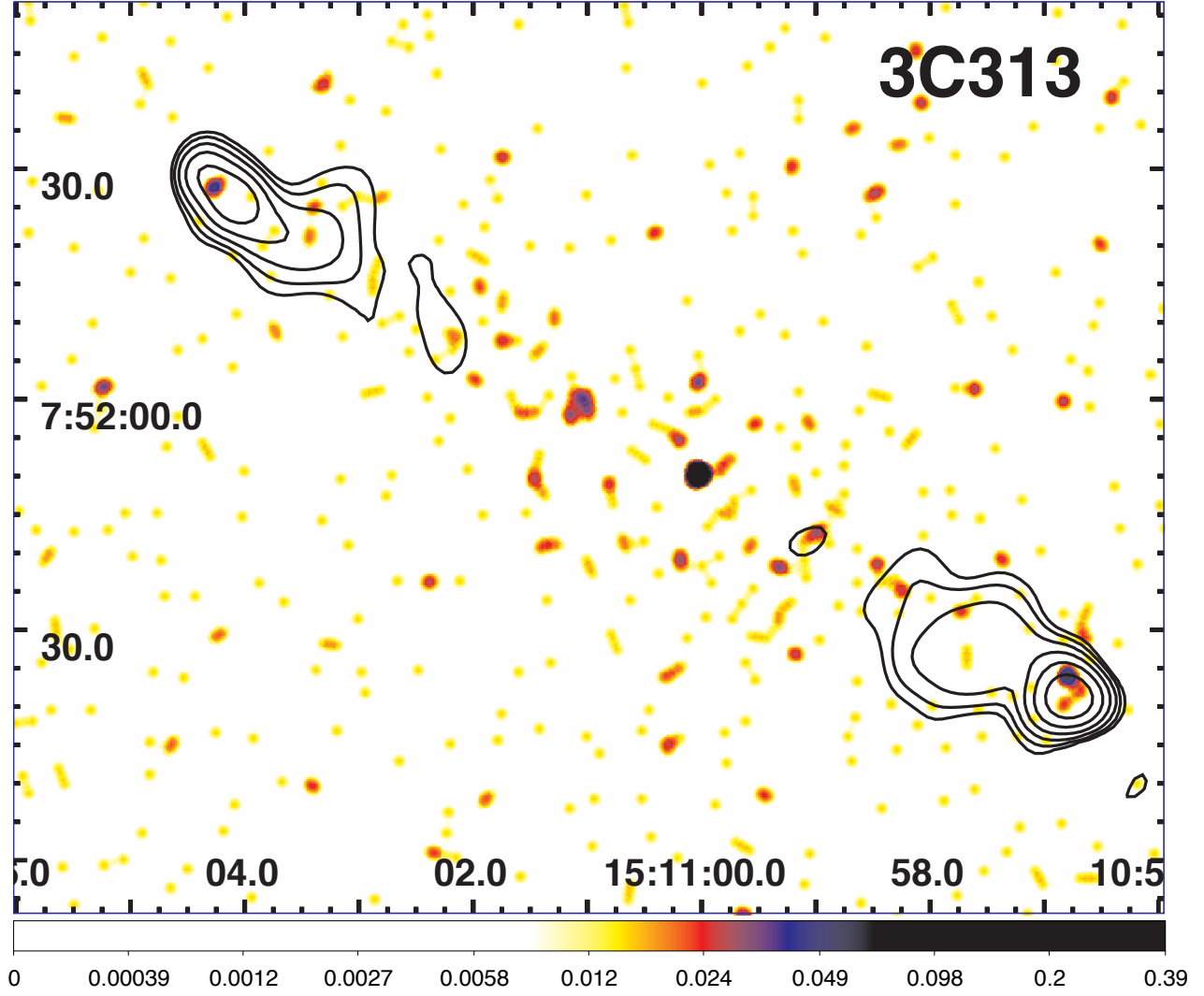


FIG. 16.— The X-ray image of 3C 313 for the energy band 0.5-7 keV. The event file has been regridded to a pixel size of $0.246''$ and smoothed with a Gaussian of $\text{FWHM}=2.0''$. The radio contours (black) come from a 1.4 GHz map constructed from archival VLA data and start at 15 mJy/beam, increasing by factors of two. The clean beam is $5''$. The VLA image at 1.4 GHz have been obtained via AIPS standard reduction procedure (<http://www.aips.nrao.edu/cook.html>).

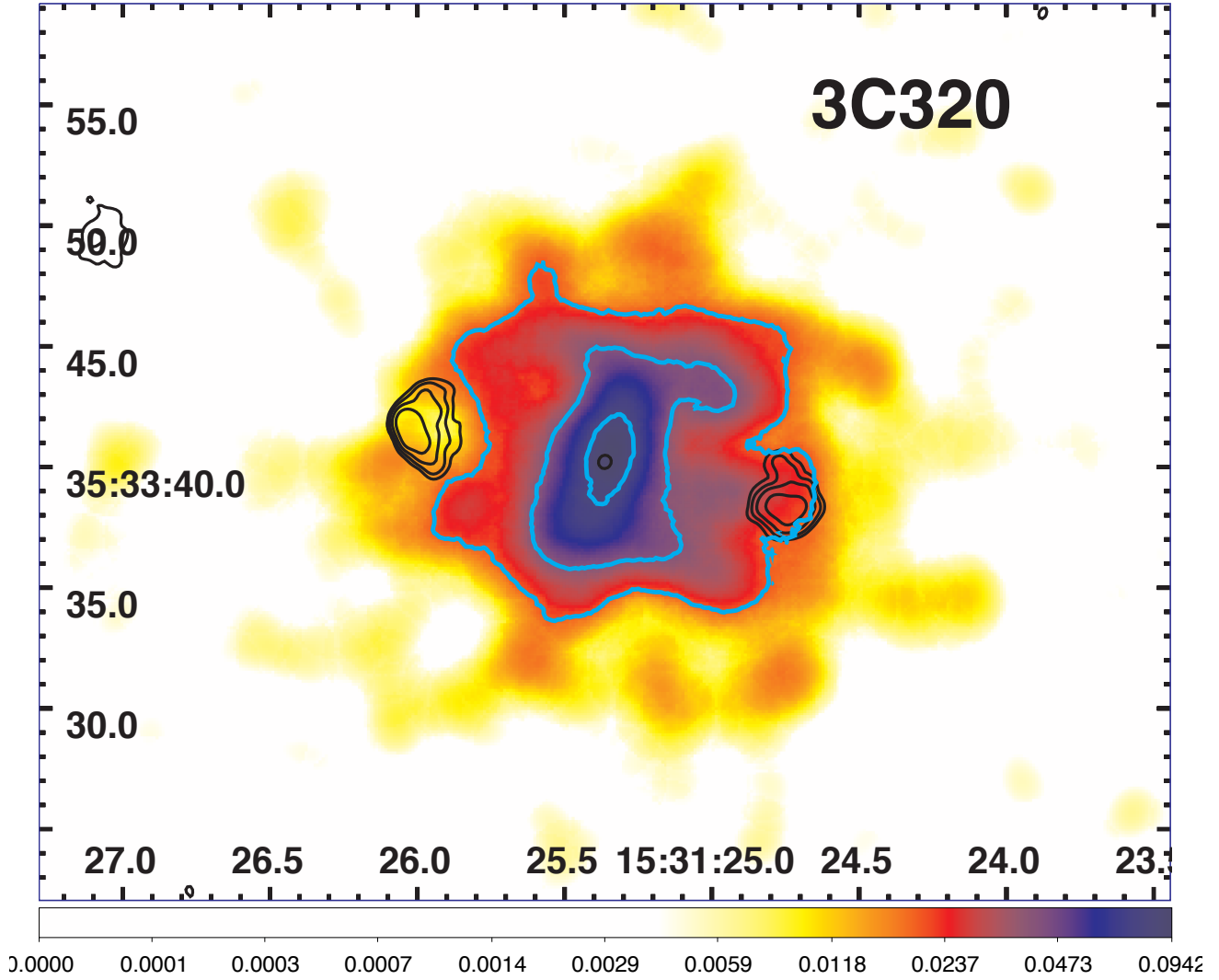


FIG. 17.— The X-ray image of 3C 320 for the energy band 0.5-7 keV. The event file has been regridded to a pixel size of $0.123''$ and smoothed with a Gaussian of $\text{FWHM}=2.5''$. X-ray contours (white or cyan) start at 0.02 counts/pix and increase by factors of two. The radio contours (black) come from a 4.9 GHz map downloaded from the NVAS and start at 0.5 mJy/beam, increasing by factors of two. The clean beam is $0.40'' \times 0.36''$ with major axis in $\text{PA}=-47^\circ$.

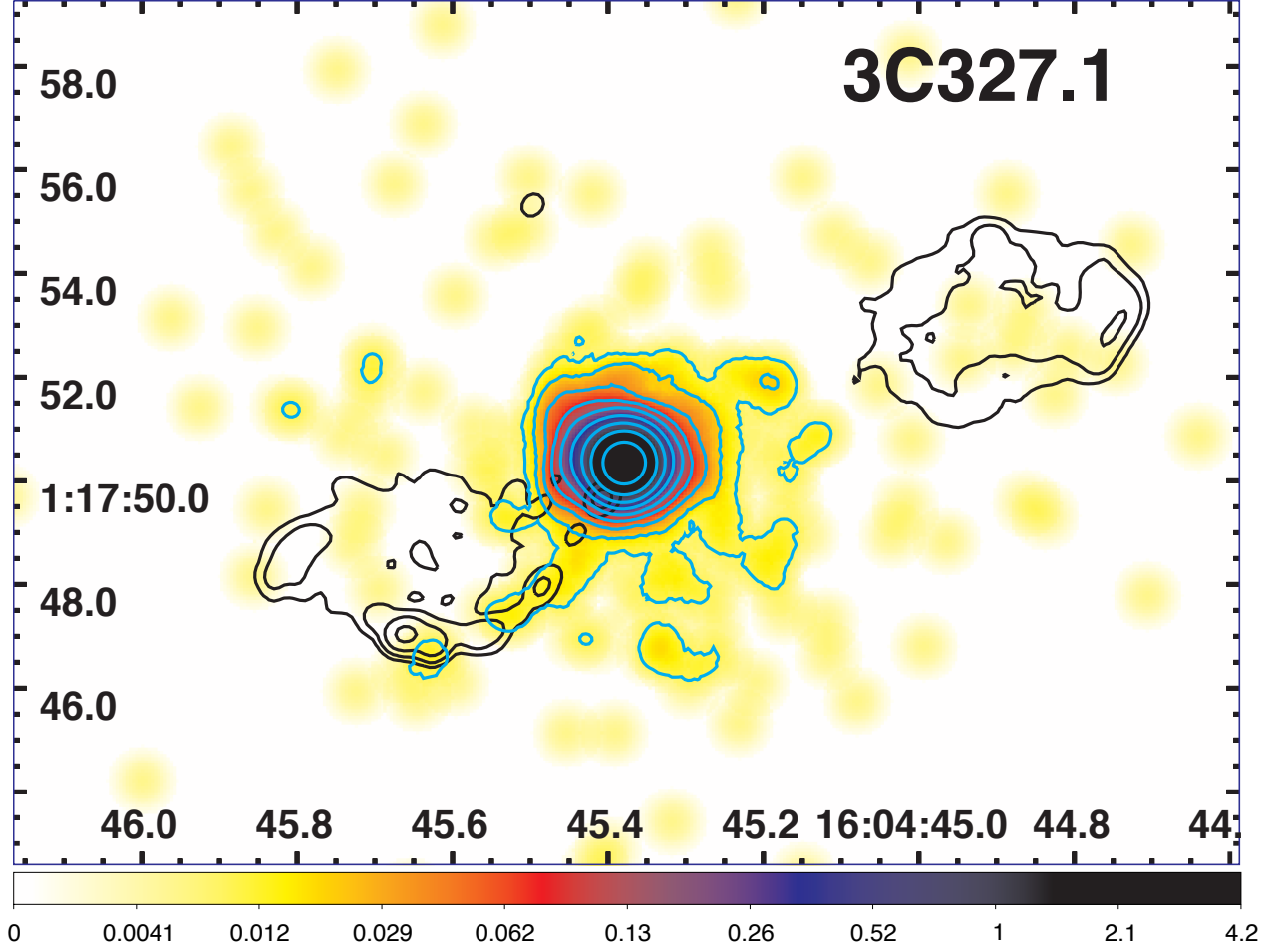


FIG. 18.— The X-ray image of 3C 327.1 for the energy band 0.5–7 keV. The event file has been regridded to a pixel size of $0.0615''$ and smoothed with a Gaussian of $\text{FWHM}=0.8''$. X-ray contours (white or cyan) start at 0.01 counts/pix and increase by factors of two. The radio contours (black) come from a 4.9 GHz map kindly supplied by R. Morganti and start at 1 mJy/beam, increasing by factors of four. The clean beam is $0.39'' \times 0.36''$ with major axis in $\text{PA}=-38^\circ$. As indicated by the lowest X-ray contour, the S jet seems to be marginally detected.

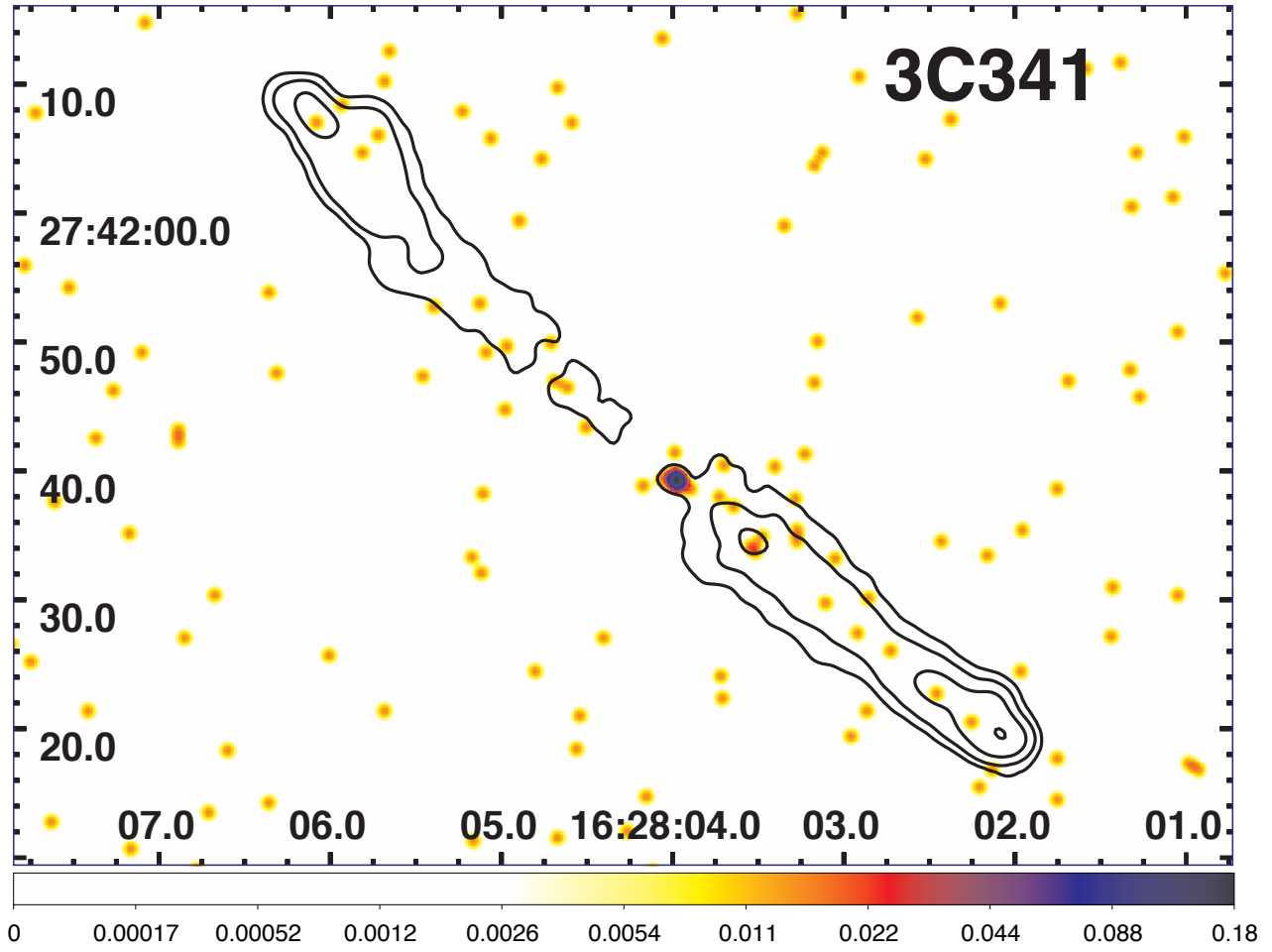


FIG. 19.— The X-ray image of 3C 341 for the energy band 0.5-7 keV. The event file has been regridded to a pixel size of $0.123''$ and smoothed with a Gaussian of $\text{FWHM}=1.0''$. The radio contours (black) come from an 8.5 GHz map kindly supplied by M. J. Hardcastle (Gilbert et al. 2004) and start at 0.25 mJy/beam, increasing by factors of four. The clean beam is $1.5''$.

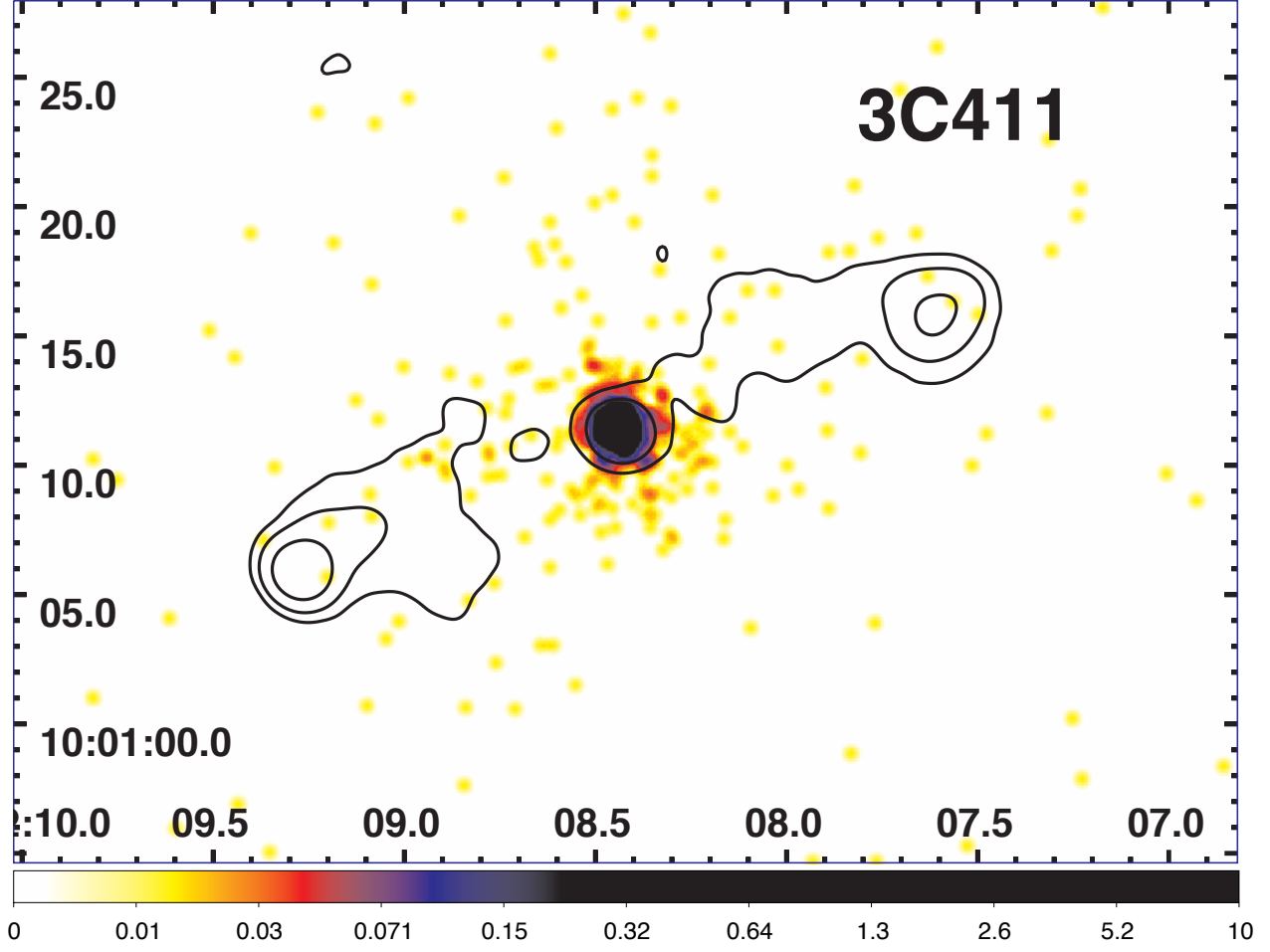


FIG. 20.— The X-ray image of 3C 411 for the energy band 0.5–7 keV. The event file has been regridded to a pixel size of $0.0615''$ and smoothed with a Gaussian of $\text{FWHM}=0.5''$. The radio contours (black) come from a 4.9 GHz map downloaded from NED and start at 4 mJy/beam, increasing by factors of four. The clean beam is $1.6'' \times 1.5''$ with major axis in $\text{PA}=57^\circ$.

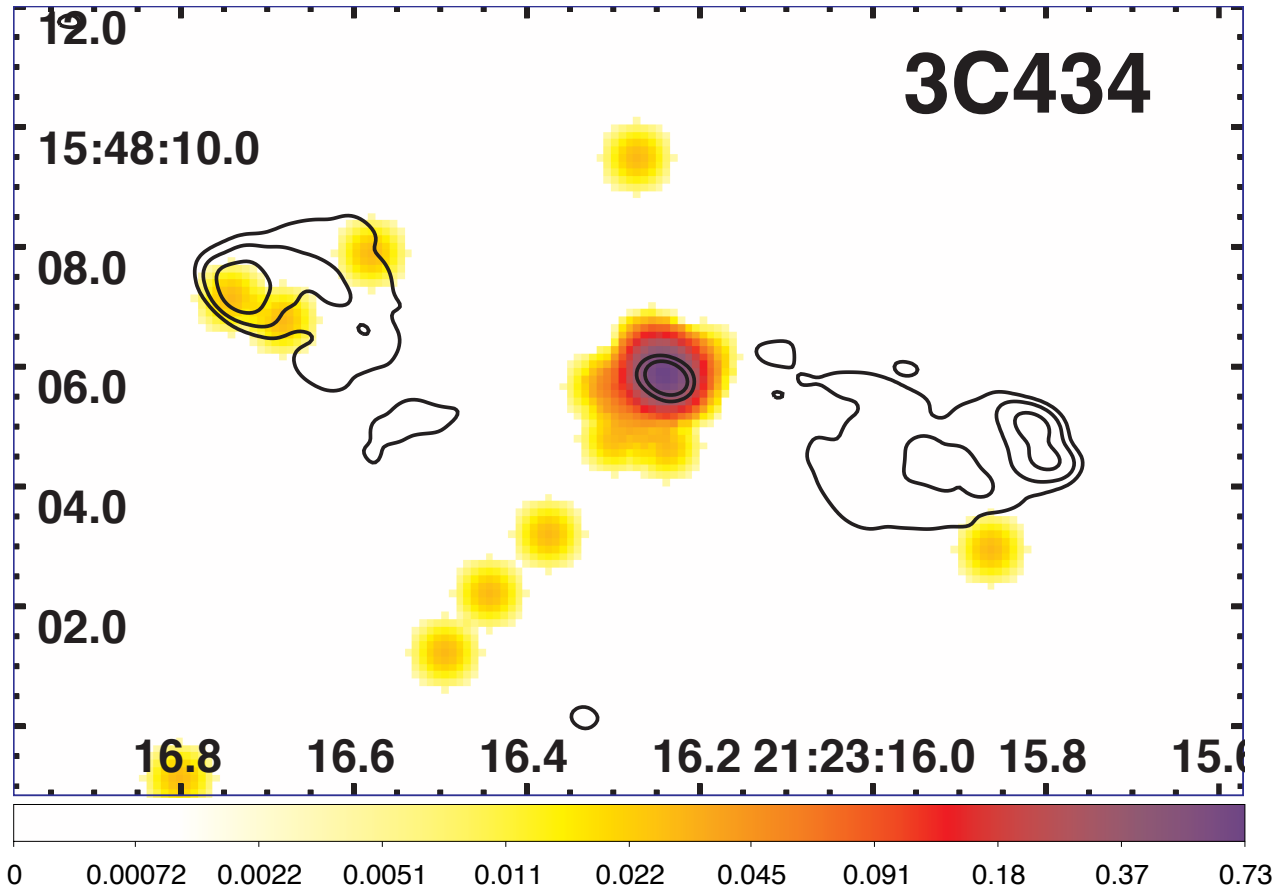


FIG. 21.— The X-ray image of 3C 434 for the energy band 0.5-7 keV. The event file has been regridded to a pixel size of $0.123''$ and smoothed with a Gaussian of $\text{FWHM}=0.72''$. The radio contours (black) come from a 4.9 GHz map constructed from archival VLA data and start at 0.5 mJy/beam, increasing by factors of four. The clean beam is $0.54'' \times 0.38''$ with major axis in $\text{PA}=66^\circ$. The VLA image at 4.9 GHz have been obtained via AIPS standard reduction procedure (<http://www.aips.nrao.edu/cook.html>).

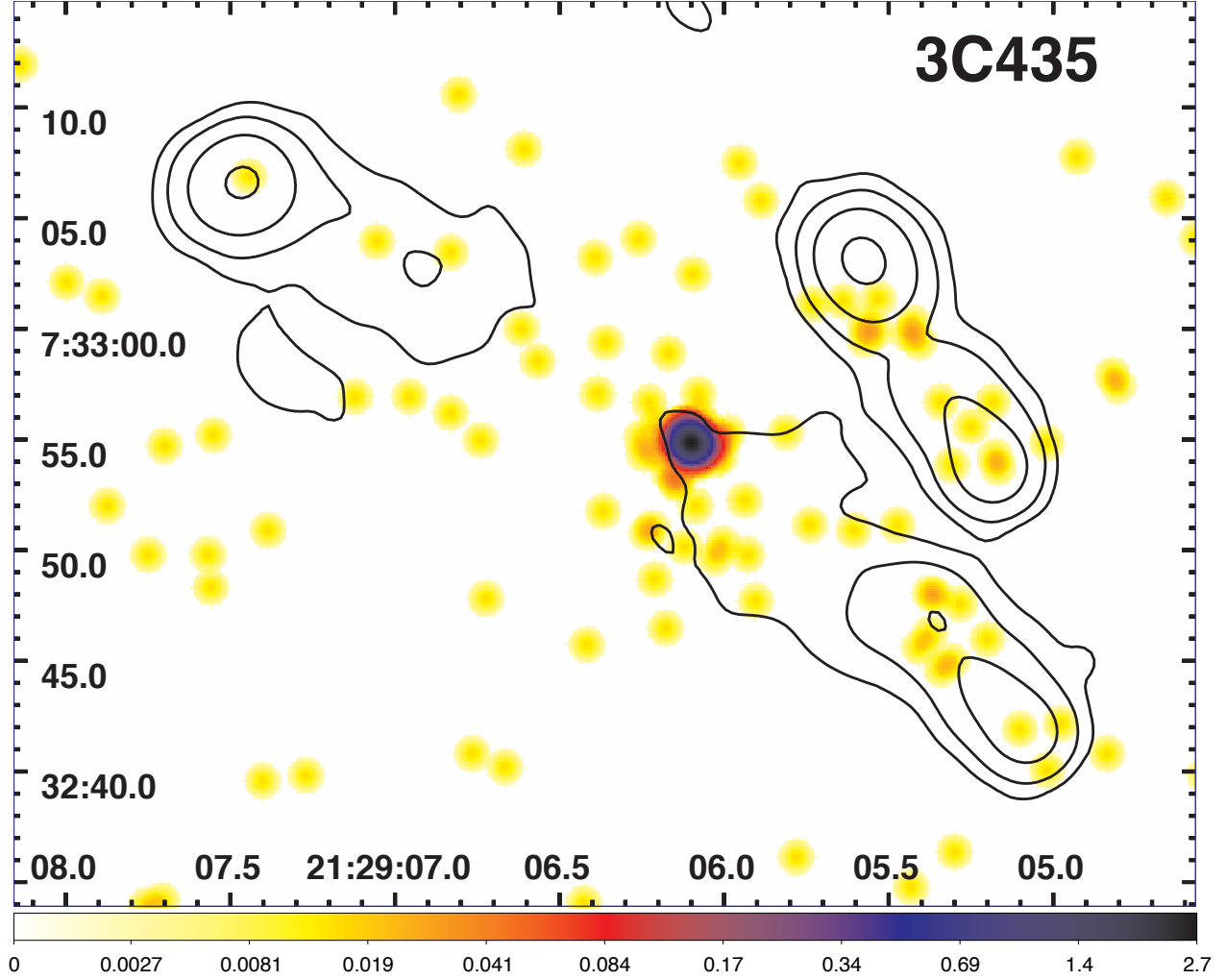


FIG. 22.— The X-ray image of 3C 435 for the energy band 0.5–7 keV. The event file has been regridded to a pixel size of $0.123''$ and smoothed with a Gaussian of $\text{FWHM}=1.0''$. The radio contours (black) come from a 1.4 GHz map downloaded from NED and start at 4 mJy/beam, increasing by factors of four. The clean beam is $2.6''$. There are two FRII radio galaxies in proximity (see McCarthy et al. 1989, for more details). X-ray emission was detected from the nucleus of the SE source (i.e., 3C 435B, ≈ 300 counts), aligned with an unresolved radio component at 5 GHz. The NW radio galaxy (i.e., 3C 435A Spinrad et al. 1985), is not detected in the *Chandra* snapshot observation.